AGU PUBLICATIONS

JGR

Journal of Geophysical Research: Atmospheres

RESEARCH ARTICLE
10.1002/2013JD021279

Key Point:
- Remote sensing of AOT is very useful in validation of climate models

Correspondence to:
P. Glantz,
paul.glantz@itm.su.se

Citation:
Glantz, P., et al. (2014), Remote sensing of aerosols in the Arctic for an evaluation of global climate model simulations, *J. Geophys. Res. Atmos.*, *119*, 8169–8188, doi:10.1002/2013JD021279.

Received 9 DEC 2013
Accepted 5 JUN 2014
Accepted article online 10 JUN 2014
Published online 2 JUL 2014

Remote sensing of aerosols in the Arctic for an evaluation of global climate model simulations

Paul Glantz[1], Adam Bourassa[2], Andreas Herber[3], Trond Iversen[4,5], Johannes Karlsson[6], Alf Kirkevåg[5], Marion Maturilli[3], Øyvind Seland[5], Kerstin Stebel[7], Hamish Struthers[8], Matthias Tesche[1], and Larry Thomason[9]

[1]Department of Applied Environmental Science, Stockholm University, Stockholm, Sweden, [2]Institute of Space and Atmospheric Studies, University of Saskatchewan, Saskatoon, Saskatchewan, Canada, [3]Alfred Wegener Institute for Polar and Marine Research, Bremerhaven, Germany, [4]ECMWF, Reading, UK, [5]Norwegian Meteorological Institute, Oslo, Norway, [6]Department of Meteorology, Stockholm University, Stockholm, Sweden, [7]Norwegian Institute for Air Research, Oslo, Norway, [8]National Supercomputer Centre, Linköping University, Linköping, Sweden, [9]NASA Langley Research Center, Hampton, Virginia, USA

Abstract In this study Moderate Resolution Imaging Spectroradiometer (MODIS) Aqua retrievals of aerosol optical thickness (AOT) at 555 nm are compared to Sun photometer measurements from Svalbard for a period of 9 years. For the 642 daily coincident measurements that were obtained, MODIS AOT generally varies within the predicted uncertainty of the retrieval over ocean ($\Delta AOT = \pm 0.03 \pm 0.05 \cdot AOT$). The results from the remote sensing have been used to examine the accuracy in estimates of aerosol optical properties in the Arctic, generated by global climate models and from in situ measurements at the Zeppelin station, Svalbard. AOT simulated with the Norwegian Earth System Model/Community Atmosphere Model version 4 Oslo global climate model does not reproduce the observed seasonal variability of the Arctic aerosol. The model overestimates clear-sky AOT by nearly a factor of 2 for the background summer season, while tending to underestimate the values in the spring season. Furthermore, large differences in all-sky AOT of up to 1 order of magnitude are found for the Coupled Model Intercomparison Project phase 5 model ensemble for the spring and summer seasons. Large differences between satellite/ground-based remote sensing of AOT and AOT estimated from dry and humidified scattering coefficients are found for the subarctic marine boundary layer in summer.

1. Introduction

Due to the ice-albedo feedback the Arctic region is estimated to be particularly sensitive to global warming [*Arctic Climate Impact Assessment*, 2005]. The warming is expected to result from a combination of increased greenhouse gas concentrations and positive feedbacks involving sea ice, snow, water vapor, and clouds [*Stroeve et al.*, 2012]. The sea ice retreat has continued for more than a decade and shows no sign of stagnation. The ice melting during summer of 2012 was even more pronounced than the previous record year 2007. *Zhang et al.* [2012] estimate the 2012 Arctic summer sea ice volume to be approximately 40% lower than the 2007–2011 mean. Snow on the surrounding land areas is also melting earlier in spring. Global climate models (GCMs) have for many years predicted a decline in Arctic perennial sea ice; nevertheless, none of the simulations capture the very fast ice retreat that has been observed [*Stroeve et al.*, 2007]. Even so, *Stroeve et al.* [2012] have shown that for the ensemble mean, simulated trends with the latest generation of GCMs are more consistent with observations over the satellite era (1979–2011).

Due to larger areas of open water in the Arctic, emissions of sea-salt and organic aerosols as well as dimethyl sulfide (DMS) are expected to increase in future [*Nilsson et al.*, 2001]. To accurately estimate the impacts on the radiation balance with regional and global climate models it is important to include these sources of aerosols in the simulations [e.g., *Struthers et al.*, 2011]. However, in order to obtain accurate model estimates of aerosol properties in the Arctic it is crucial to understand the seasonal variability. Useful parameters for this purpose are optical parameters that have been regularly observed from both ground [*Holben et al.*, 1998] and space [e.g., *Levy et al.*, 2010; *Kahn et al.*, 2011] for over a decade. Simulations of aerosol optical properties have been performed with the CMIP5 (fifth phase of Coupled Model Intercomparison Project) version of the Norwegian Earth System Model (NorESM1-M) [*Bentsen et al.*, 2013; *Iversen et al.*, 2013], with atmospheric module Community Atmosphere Model (CAM) version 4 Oslo [*Kirkevåg et al.*, 2013]. In a work by *Struthers et al.* [2011],

the NorESM predecessor atmospheric model CAM-Oslo (based on CAM3) was forced using sea ice concentrations consistent with present-day conditions for the Arctic region and projections of sea ice extent for the year 2100. The simulated sea-salt aerosol emissions increased in response to a decrease in sea ice. The increase in emissions in turn leads to an increase in the natural aerosol optical thickness (AOT) of approximately 23% [*Struthers et al.*, 2011]. However, biases in Arctic atmospheric circulation in CAM3 have previously been reported [e.g., *Hurrell et al.*, 2006; *Hack et al.*, 2006; *Deweaver and Bitz*, 2006], which may influence the meridional transport of aerosols into the Arctic region. Therefore, it is important to validate the simulation of the Arctic aerosol from regional and global climate models against observations.

Sea-salt aerosol is the dominant primary aerosol source over open oceans [*Lewis and Schwartz*, 2004]. Previous studies performed at Barrow, Alaska, [*Quinn et al.*, 2002] and the Zeppelin mountain station, Svalbard, [*Weinbruch et al.*, 2012] as well as in the Norwegian Arctic [*Pacyna and Ottar*, 1985] suggest that sea salt contributes considerably to the Arctic aerosol. In addition, *Quinn et al.* [2002] found that the concentration of supermicron sea-salt aerosol peaks in summer at Barrow (11 m above the mean sea level) due to the seasonal decrease in sea ice extent. At this station, sea salt together with particulate sulfate was found to control light scattering in summer. In addition, significant fractions of the total mass concentrations measured in summer at the Zeppelin mountain station (474 m above mean sea level (asl)) correspond to sea salt-related ions [*Zieger et al.*, 2010]. However, previous studies have found relatively strong vertical gradients in sea-salt aerosol concentrations in the lower troposphere [*Clarke et al.*, 1996; *Gong et al.*, 1997; *Glantz et al.*, 2004; *Reid et al.*, 2006; *Textor et al.*, 2006; *Lundgren et al.*, 2013]. There are a number of ways in which the vertical transport of sea-salt particles can be reduced or even eliminated—one of which is boundary layer decoupling [*Nicholls*, 1984; *Bretherton et al.*, 1995; *Johnson et al.*, 2000; *Osborne et al.*, 2000; *Wood et al.*, 2000]. Relatively strong vertical gradients have also been observed and modeled for coarse mode ($>1\ \mu$m radius) aerosols, and modeled for submicron aerosols, in otherwise well-mixed marine boundary layers (MBLs) without thermodynamic evidence of decoupling [*Glantz et al.*, 2004].

Observations of aerosol microphysical properties as well as sulfur dioxide and carbon monoxide at the Zeppelin station can be used to provide an indication of changes in air mass transport in the Arctic region [see *Engvall et al.*, 2008]. In that study of the years 2000–2005 it was concluded that changes in source strength and transport of air masses are important for the annual variations of aerosol properties in the Arctic. However, these factors could not fully explain the observed rapid changes from spring to summer. It was suggested that important factors for new particle formation during the Arctic summer period are higher insolation, hence higher levels of OH, combined with a decreased condensation sink, caused by more efficient precipitation scavenging of preexisting aerosol surface area [*Engvall et al.*, 2008]. Observations of aerosol size distribution both at the Zeppelin station and Barrow, Alaska, show that accumulation mode particles dominate the aerosol distribution during winter and spring while Aitken mode particles dominate in summer [*Bodhaine et al.*, 1981; *Bodhaine*, 1989; *Quinn et al.*, 2002; *Ström et al.*, 2003; *Engvall et al.*, 2008]. Furthermore, measurements of scattering coefficients of dehydrated aerosol particles performed with a nephelometer at the two Arctic stations consequently revealed very low values in summer (less than 2 M m^{-1}) [*Quinn et al.*, 2002; *Tomasi et al.*, 2007]. Note that this occurs at the same time as the relative humidity (RH) is high (70–90%) in the lower summer troposphere [*Treffeisen et al.*, 2007a; *Zieger et al.*, 2010]. This means that the ambient aerosol scattering coefficients in the Arctic summer are substantially higher (by a factor of 3.2 at RH = 85% [*Zieger et al.*, 2010]) than the dry in situ scattering coefficients.

Based on continuous aerosol optical observations from the Koldewey station in Ny-Ålesund, Svalbard, a clear annual variation is apparent in tropospheric ambient AOT over the period 1991 to 1999 [*Herber et al.*, 2002]. The stratospheric contribution of AOT was obtained from the Stratospheric Aerosol Gas Experiment (SAGE II) [*Russell and McCormick*, 1989; *Kent et al.*, 1994]. A transition from higher AOTs during spring to low summer values occurred over a short period between May and June. Furthermore, *Toledano* [2012] have found substantially higher monthly summertime mean AOTs at Svalbard for the period 2002–2010 compared to the 1990s [*Herber et al.*, 2002]. However, *Toledano* [2012] did not aim to describe a local background situation. In fact, during the time period under consideration, the Arctic was highly influenced in July 2004 by aerosols from boreal fires in Canada [*Stohl et al.*, 2006] and from the Kasatochi and Sarychev volcanic eruptions, which were starting in August 2008 [*Hoffmann et al.*, 2010] and July 2009 [*Tomasi et al.*, 2012], respectively.

Glantz and Tesche [2012] showed that satellite retrievals of column AOT, based on Moderate resolution Imaging Spectroradiometer collection 5 (hereafter referred as MODIS) [*Remer et al.*, 2005], agree well with

Aerosol Robotic Network (AERONET) [*Holben et al.*, 1998] observations in Europe. The AOT values were found to vary within the expected uncertainty range of the MODIS retrieval over land. The predicted uncertainty ranges of the satellite retrievals are lower over the ocean [*Remer et al.*, 2005], where the surface reflection is substantially lower than for land surfaces. Estimates of AOT are not available with the MODIS algorithm directly over snow and ice, since the surface reflection is high. Methods to retrieve AOT from satellite data over snow and ice have only recently been developed [*Istomina et al.*, 2011; *Mei et al.*, 2013a, 2013b]. Although promising results were obtained from these studies, AOT data are available only for limited time periods and with high bias. Consequently, it is not yet possible to perform spaceborne investigations of polar AOT over bright surfaces at a quantitative level.

In the present study 9 years of MODIS observations are combined with ground-based long-term Sun photometer measurements and climate model simulations to examine the accuracy in estimates of aerosol optical properties (i.e., AOT and scattering coefficient) in the Arctic marine atmosphere. In addition, aerosol remote sensing is combined with dry and wet nephelometer in situ measurements at the Zeppelin station, Svalbard. The following questions are addressed:

1. How representative are spatial averages of MODIS AOT over ocean areas around Svalbard in comparison to ground-based Sun photometer observations?
2. How accurately does the NorESM1-M/CAM4-Oslo global climate model simulate AOT for the Svalbard area?
3. How representative are in situ measurements of dry and wet aerosol scattering coefficients for actual atmospheric conditions in the subarctic marine boundary layer?

2. Aerosol Optical and Microphysical Data and Model Configuration

2.1. Remote Sensing

2.1.1. MODIS Nadir View Over Ocean

In the present study, we use the MODIS Aqua Collection 5 level 2 standard products for best quality retrievals (quality flag = 3) over ocean surfaces. Data were taken from the NASA Goddard Space Flight Center's Atmosphere Archive and Distribution System (http://ladsweb.nascom.nasa.gov). A detailed description of the MODIS ocean algorithm can be found in *Remer et al.* [2005]. After the water vapor, ozone and carbon dioxide corrections have been applied the next step in the algorithm is to organize the reflectance at six wavelengths into 10 km^2 boxes of 20×20 pixels at 500 m horizontal resolution. The ocean algorithm requires that all 400 pixels in the box are identified as ocean pixels. If any land is encountered the entire box is handled by the land algorithm. The cloud screening is performed individually for the 400 pixels [*Gao et al.*, 2002; *Martins et al.*, 2002]. Pixels that remain in a 10 km^2 box after cloud screening are sorted according to their 858 nm brightness. The darkest and brightest 25% of the pixels are discarded, thereby leaving 50% of the cloud-free data for the retrieval. AOT is retrieved if at least 10 of the 400 pixels in the original box remain after masking and filtering.

The MODIS ocean retrieval gives AOT at 555 nm with an estimated error of $\Delta\mathrm{AOT} = \pm 0.03 \pm 0.05 \cdot \mathrm{AOT}$ [*Remer et al.*, 2005]. We use MODIS AOTs at wavelengths $\lambda 1 = 555$ nm and $\lambda 2 = 858$ nm to calculate the Ångström exponent [*Ångström*, 1964] α:

$$\alpha = -\frac{1\mathrm{n}\frac{\mathrm{AOT}_{\lambda 1}}{\mathrm{AOT}_{\lambda 2}}}{1\mathrm{n}\frac{\lambda_1}{\lambda_2}} \tag{1}$$

Since MODIS retrievals of AOT is not available directly over Svalbard, a larger area (75°N–82°N, 10°W–40°E) has been introduced in the averaging of the aerosol optical properties. If the satellite mean AOT values obtained can be considered as representative for the measurement stations at Svalbard, which requires homogeneous aerosol conditions, this approach improves the availability of AOT observations in the region and complements ground-based Sun photometer measurements. However, due to the polar nights the passive MODIS sensor and Sun photometers (section 2.1.2) used here only produce data during about half of the year. In the present study, one satellite scene per day is included in the analysis for the days with cloud-free conditions over the investigation area during the analysis period (2003–2011).

Figures 1a and 1b show satellite scenes of MODIS AOT at the wavelength 555 nm over the Greenland Sea and the Barents Sea for 7 July 2005 and 2 May 2006, respectively. Aerosols were rather homogenously

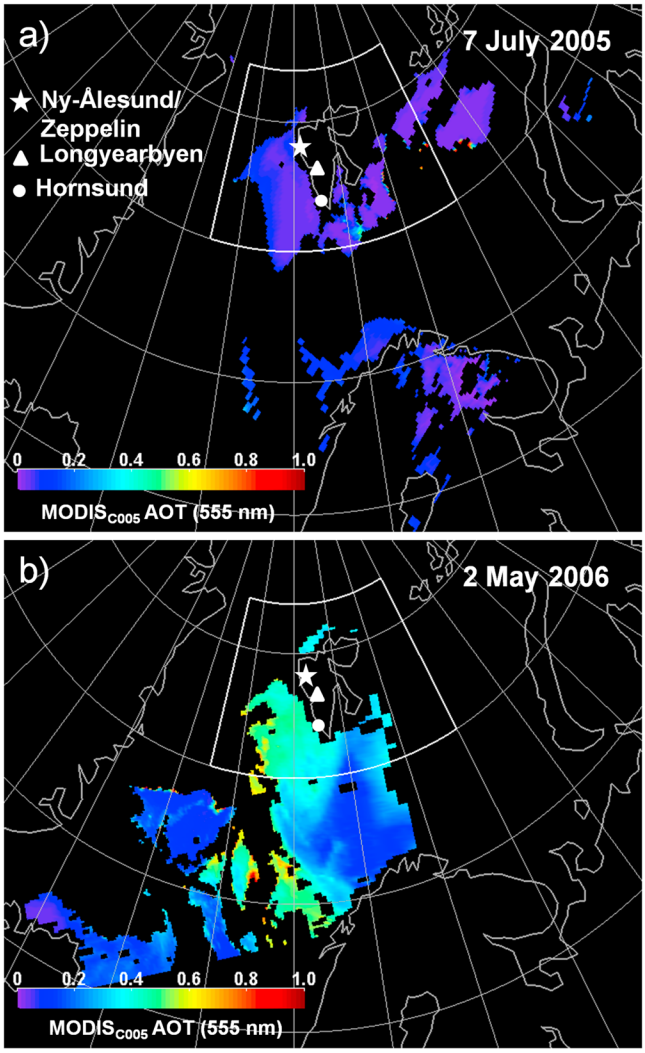

Figure 1. MODIS Aqua scenes of AOT at 555 nm for two overpasses: (a) in summer and (b) in spring. The white box in each figure denotes the area (75°N–82°N, 10°W–40°E) used for the averaging of MODIS retrieved and model-simulated aerosol optical parameters. The locations of the ground-based Sun photometer stations Ny-Ålesund (78.9°N, 11.9°E, marked with a star), Longyearbyen (78.2°N, 15.6°E, triangle), and Hornsund (77.0°N, 15.6°E, circle) as well as the Zeppelin in situ measurement station (78.9°N, 11.9°E, marked with a star) are also shown.

distributed during summer background condition (Figure 1a), while larger spatial variation occurred when the investigation area (white box) was influenced by continental aerosols from midlatitudes in spring (Figure 1b). In May 2006, agricultural fires in Eastern Europe resulted in record high pollution levels (e.g., ~0.6 in AOT at 442 nm) in the Arctic region [e.g., *Stohl et al.*, 2007; *Myhre et al.*, 2007; *Treffeisen et al.*, 2007b]. Note that problems with cloud screening (i.e. spots of increased AOT in Figure 1a) occur in the transition area, between cloud and aerosol fields. To exclude these cloud-contaminated pixels, we excluded all pixels with AOT $>$ 0.5 for cases with daily mean AOT $<$ 0.07. This additional cloud screening has minor influence on mean and median values but strongly decreases the corresponding standard deviation. Based on relative frequency histograms of AOT (500 nm) from Sun photometer measurements at Ny-Ålessund during the period 1999–2010 a threshold value of 0.08 for the summer background aerosol has been estimated by *Tomasi et al.* [2012]. *Herber et al.* [2002] found that more than 90% of the AOT (532 nm) values measured at Ny-Ålesund in the 90s were between 0.022 and 0.070 in summer.

2.1.2. Sun Photometer Measurements at Svalbard

MODIS AOT retrieved over the Arctic Ocean has been compared to AERONET level 2.0 data (quality assured) from Longyearbyen (78.2°N, 15.6°E, 30 m asl) and Hornsund (77.0°N, 15.6°E, 10 m asl), Svalbard, for the periods 2003–2004 and 2005–2011, respectively. Information about the CIMEL Sun photometers operated at these sites can be found at http://aeronet.gsfc.nasa.gov. AERONET data used for this study include AOT at 500 nm as well as the Ångström exponent α (440/675 nm). These values were recorded every 15 min and automatically cloud screened [*Smirnov et al.*, 2000]. AERONET-derived estimates of spectral AOT are expected to be accurate within ±0.01 for wavelengths larger than 440 nm [e.g., *Holben et al.*, 1998].

Since 1991 AOT measurements are also performed at Koldewey station (78.9°N, 11.9°E, 20 m asl), Ny-Ålesund, by the Alfred Wegener Institute (AWI), Potsdam, Germany. The AOT is measured during daylight conditions with a Sun photometer of type SP1A (Dr. Schulz and Partner GmbH, Buckow, Germany, http://www.drschulz.com/). Due to low aerosol loading in the polar regionaccuracy requirements for AOT measurements are more stringent than those performed in other regions (see the recommendation of the Polar Aerosol Optical Depth Measurement (POLAR-AOD) intercomparison campaign [*Mazzola et al.*, 2012]). Ny-Ålesund is part of the Polar Aerosol Optical

Depth Measurement (POLAR-AOD) Sun photometer network, which was founded to organize Sun photometer measurements in polar region to identify trends and regional differences. Due to regular intercomparison campaigns the quality of measurements are guaranteed and data at different stations are directly comparable. The network was an initiative within the activity of the International Polar Year 2007–2009 [see *Mazzola et al.*, 2012; *Tomasi et al.*, 2007, 2012]. AWI-AOD data used for the present study include AOT at 501 nm as well as the Ångström exponent α (501/610 nm).

The locations of the ground-based Sun photometer stations Longyearbyen, Hornsund, and Ny Ålesund are shown in Figure 1. For the days when the Sun photometers were in operation mode during the current investigation period (2003–2011) all quality assured data values from AERONET and AWI-AOD network are included in the present study.

2.1.3. Aerosol Data From Stratospheric Aerosol and Gas Experiment III and Odin-Osiris

Total column AOT from Sun photometer measurements can be converted to tropospheric AOT if the aerosol loading in the stratosphere is known. This information is provided, i.e., by the Stratospheric Aerosol and Gas Experiment III (SAGE III) [*Thomason et al.*, 2010] and the Optical Spectrograph and Infrared Imaging System (OSIRIS) [*Murtagh et al.*, 2002] instruments. SAGE III is a solar occultation instrument that was launched in December 2001 aboard the Russian METEOR 3M spacecraft. Data were acquired from February 2002 until March 2006. An ensemble of line-of-sight transmission profiles in the wavelength range from the ultraviolet to the infrared is used to produce vertical profiles of aerosol extinction coefficients at nine wavelengths [*Stratospheric Aerosol and Gas Experiment III Algorithm Theoretical Basis Document*, 2002; *Thomason et al.*, 2010]. *Thomason et al.* [2010] find aerosol extinction data at 520 and 755 nm to be accurate to 10% throughout the lower stratosphere. An approximate stratospheric AOT is obtained here by integrating the aerosol extinction coefficient in the height range from 12 to 40 km. We use stratospheric AOT at 520 and 755 nm for zonal means between 43°N and 80°N and use these values to calculate the α_{SAGE} according to equation (1).

The limb-scanning OSIRIS instrument aboard the Swedish satellite Odin was designed to measure the vertical profile of atmospheric limb radiance spectra at wavelengths from 274 nm to 810 nm. The satellite was launched into a Sun-synchronous polar orbit on 20 February 2001 and continues in full operation to the present date. Hence, OSIRIS provides a time series that now spans over more than a decade of observations. The OSIRIS stratospheric aerosol retrieval was developed by *Bourassa et al.* [2007, 2008]. The OSIRIS version 5 data product includes vertical profiles of the approximate stratospheric aerosol extinction coefficient at 750 nm [*Bourassa et al.*, 2012a]. As for SAGE III, approximate stratospheric AOT is determined by integrating the aerosol extinction coefficient between 12 and 40 km height. We use zonal mean AOTs at 750 nm for the latitude range from 75°N to 85°N. The α_{SAGE} was applied to OSIRIS data to estimate AOT at 555 nm for the period 2003 to 2011. For further details on OSIRIS and Odin, see *Llewellyn et al.* [2004] and *Murtagh et al.* [2002], respectively.

2.2. In Situ Nephelometer and Differential Mobility Particle Sizer Measurements

In situ data from Zeppelin station (78.9°N, 11.9°E, 474 m asl) include the aerosol scattering coefficient and the aerosol size distribution. A nephelometer (TSI Inc., Model 3563) is used to measure the scattering coefficient at the wavelengths of 450, 550, and 700 nm under dry conditions with RH $<$ 20% [*Ström et al.*, 2003]. The nephelometer measures within scattering angles from 7° to 170°, and values for the complete scattering range from 0° to 180° were retrieved by the truncation error correction proposed by *Anderson and Ogren* [1998]. Dry scattering coefficients are transformed to ambient conditions using a median fit parameter of $\gamma = 0.57$ for the parameterization of the scattering enhancement factor $f(\mathrm{RH}) = (1 - \mathrm{RH})^{-\gamma}$ according to *Zieger et al.* [2010]. Coincident observations with a Particle Soot Absorption Photometer showed that the contribution of absorption to the ambient extinction coefficient at Zeppelin is negligible. The aerosol size distribution is measured using a Differential Mobility Particle Sizer (DMPS), which scans in size bins from 10 to 794 nm diameter. ATSI 3010 Condensation Particle Counter is used for successive counting. The time resolution of the in situ parameters analyzed here is 1 h. The location of the Zeppelin station is shown in Figure 1.

2.3. NorESM1-M/CAM4-Oslo Global Climate Model

The CMIP5 version of NorESM, NorESM1-M [*Bentsen et al.*, 2013; *Iversen et al.*, 2013], is to a large extent based on the Community Climate System Model (CCSM4.0) [*Gent et al.*, 2011; *Meehl et al.*, 2012]. The sea ice and land

models (Community Ice Code version 4 and Community Land Model version 4, respectively) are the same as in CCSM4.0, with the exception for a slightly different tuning of snow grain size for fresh snow on sea ice and a different treatment of deposition of aerosols on snow and sea ice (coming from CAM4-Oslo instead of prescribed fields) when the model is run fully coupled. The atmosphere module CAM4-Oslo was constructed by coupling the CAM4 general circulation model [*Neale et al.*, 2010] to a detailed module for aerosol life-cycling and aerosol cloud interactions, described in detail by *Kirkevåg et al.* [2013]. Furthermore, NorESM1-M uses the Miami Isopycnic Coordinate Ocean Model (instead of Parallel Ocean Program 2 of CCSM4.0). For this study, however, NorESM1-M was configured with CAM4-Oslo coupled to the land model and data sea ice and ocean module (an Atmospheric Model Intercomparison Project (AMIP)-type simulation with prescribed sea surface temperatures (SSTs)), using the finite volume dynamical core for transport calculations, with horizontal resolution 1.9° (latitude) × 2.5° (longitude) and a hybrid η vertical coordinate with 26 levels, as in the original CAM4 model. The model was run for the 3 years 2006–2008 with monthly prescribed observed SSTs (but without nudging), using initial boundary conditions from the end of a 1979–2005 AMIP simulation. With such a long spin-up, all three simulated years were used in the analysis. The SST and ice fraction data are from The Hadley Centre Global Sea Ice and sea surface temperature data set (1° × 1° horizontal resolution).

The CAM4-Oslo aerosol scheme includes prognostic aerosols (sulfate particulate organic carbon (including methane sulphonic acid (MSA)), black carbon, sea salt, and mineral dust) and gaseous aerosol precursors (DMS and SO_2) yielding sulfate (SO_4). The parameterizations of sea-salt emissions and aerosol processes used in the model are described by *Kirkevåg et al.* [2013]. Lookup tables for aerosol optics in the model use ambient RH and a range of process specific aerosol concentrations as input parameters. The tables are thoroughly described in *Seland et al.* [2008] and *Kirkevåg and Iversen* [2002]. The all-sky AOT was simulated at 550 nm for the current investigation area using Intergovernmental Panel on Climate Change Fifth Assessment Report (IPCC AR5) RCP8.5 aerosol emissions for the years 2006–2008 [*Lamarque et al.*, 2010], see also http://cmip-pcmdi.llnl.gov/cmip5/forcing.html. Note that emissions from eruptive volcanoes are not included in the emission inventories that were used here. For more details about the CAM4-Oslo specific natural emissions, see *Kirkevåg et al.* [2013]. See *Iversen et al.* [2013] for aerosol optical thickness, column burdens, and climate response results for the respective fully coupled NorESM1 simulation. The clear-sky AOT is estimated as all-sky optical depth weighted with the clear-sky fraction, based on total cloud cover in the model. This clear-sky definition gives larger weight to conditions for which a passive remote sensing of AOT can be made. For further details on the CAM4-Oslo model see *Kirkevåg et al.* [2013].

3. Results and Discussion

3.1. Daily Median AOT for the Years 2003–2010

Figure 2 shows MODIS median column AOT at the wavelength 555 nm, calculated for the area given in Figure 1 and Sun photometer measurements of median AOT (daily) from AERONET (Longyearbyen/Hornsund) as well as AWI-AOD (Ny-Ålesund), for the years 2003–2011. The Ångström power law (equation (1)) was used to convert AERONET and AWI-AOD 500 nm AOT to the wavelength of 555 nm for which AOT is retrieved with MODIS. The number of median values is substantially higher for MODIS than for the Sun photometer retrievals due to the strong effect of clouds on the ground-based measurements. Figure 2 reveals on the whole higher AOT in late winter/spring compared to summer. This suggests that the aerosol loading in the Arctic is occasionally enhanced by continental aerosols from midlatitudes (Arctic haze events [e.g., *Treffeisen et al.*, 2007b; *Engvall et al.*, 2008]). However, marine aerosols for which the production is driven by surface wind speed [e.g., *Nilsson et al.*, 2001; *Glantz et al.*, 2004; *Pierce and Adams*, 2006; *Mulcay et al.*, 2008; *Glantz et al.*, 2009; *Smirnov et al.*, 2012] probably also contributed significantly to the observed AOTs. The latter assumption is supported by relatively high surface wind speeds of up to 10 m s^{-1} for spring, obtained from European Centre for Medium-Range Weather Forecasts (ECMWFs) reanalysis data for the area around Svalbard (not shown). Note as well that submicron sea-salt particles have a relatively long turnover time [*Gong et al.*, 1997; *Nilsson et al.*, 2001]. This is supported by *Quinn et al.* [2002], who found that the submicron sea-salt particle mass concentrations peaked in winter and early spring at Barrow, Alaska, presumably due to long-range transport from the northern Pacific Ocean. For cloud-free conditions during spring in the period 1991–1999, *Herber et al.* [2002] estimated that the Svalbard area was influenced by Arctic haze events up to 40% of the time.

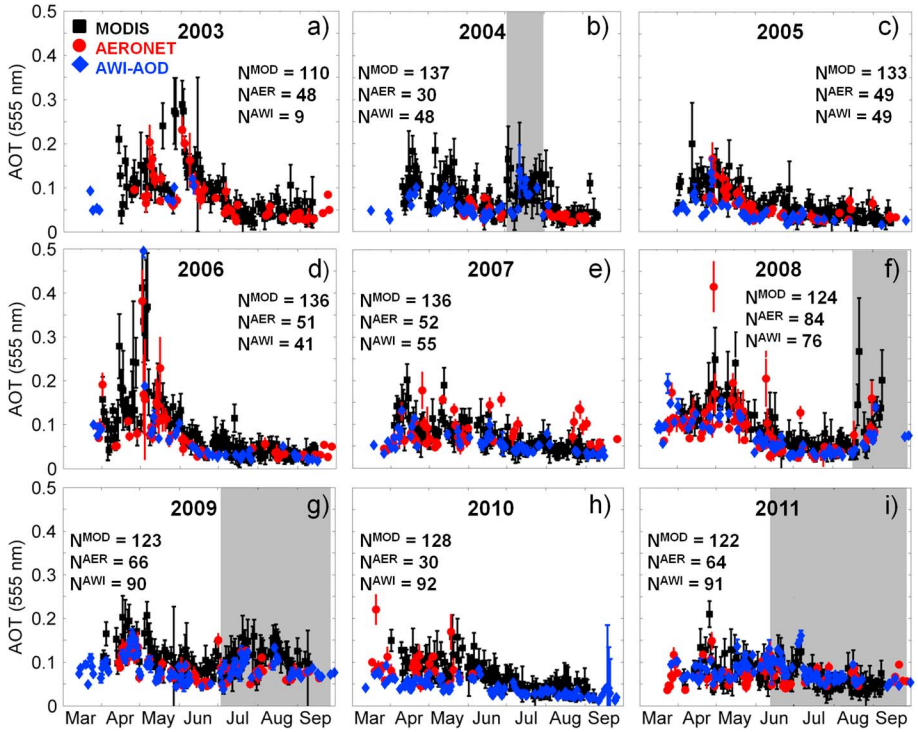

Figure 2. Median column AOT averaged on daily basis for MODIS (MOD: black square) as well as AERONET (AER: red circle) and AWI-AOD (AWI: blue diamond) observations performed during (a) 2003, (b) 2004, (c) 2005, (d) 2006, (e) 2007, (f) 2008, (g) 2009, (h) 2010, and (i) 2011. *N* denotes the number of daily median values considered for the respective year. Gray areas refer to time periods for which column AOT over the Svalbard region was influenced by long-range transport of smoke particles from Canadian forest fires in June 2004, as well as Kasatochi, Sarychev, and Nabro volcanic aerosols from 15 August 2008, 3 July 2009, and 22 June 2011, respectively.

The summer season was on the whole characterized by low AOTs that coincides with surface wind speeds of around 5.5 m s^{-1} (ECMWF). Note that long-range transport of aerosols in the free troposphere from biomass burning and volcanic eruptions sporadically influenced the AOT in the Svalbard region in summer, during some of the years considered in this study (denoted with grey areas in Figure 2). The most pronounced events were Canadian biomass-burning aerosol during July 2004 [*Stohl et al.*, 2006] and volcanic aerosol from the eruptions of Kasatochi (52.17°N, 175.51°W), Alaska, starting on 8 August 2008, and Sarychev (48.09°N, 153.20°E), Russia, starting at 12 June 2009. Aerosol layers from the Kasatochi and Sarychev eruptions have been observed with the Koldewey Aerosol Raman Lidar at Ny-Ålesund, Svalbard, between 15 August and 24 September 2008 and 3 July and early October 2009, respectively (*Hoffmann et al.* [2010] and *Tomasi et al.* [2012], respectively).

3.2. MODIS 9 Year Daily Median AOT

Figure 3 shows the seasonal variation of MODIS median column AOT at 555 nm for the period 2003–2011. With the exception of the summer season, each value has been averaged over all aerosol pixels within a satellite scene (one per day for the days that aerosol data exist) inside the area shown in Figure 1. Each value thus corresponds to 1 day of the year, averaged over the 9 years included in the present study. The summer values are assumed to represent background conditions. To obtain these values, the influences from events of forest fires and volcanic eruptions in summer, as described in the previous section, have been excluded in the calculation of median AOT. Figure 3 shows that relatively large variability in AOT occurs in spring (typical Arctic haze season), while low median values and corresponding relatively low standard deviations are found in summer and early fall (see also Table 1). This can probably be explained by a decrease in surface wind speed in summer (ECMWF, section 3.1) and consequently a decrease in emission of marine aerosols from the ocean [*Nilsson et al.*, 2001]. The Arctic is also more isolated from midlatitudinal aerosol sources during the summer season due to location of the polar front at around 70°N in summer [*Iversen and Joranger*, 1985]. Furthermore, *Serreze and Barrett* [2008] have investigated counts of closed surface low pressure centers in the Arctic over the period 1958–2005. They found that cyclonic activity in

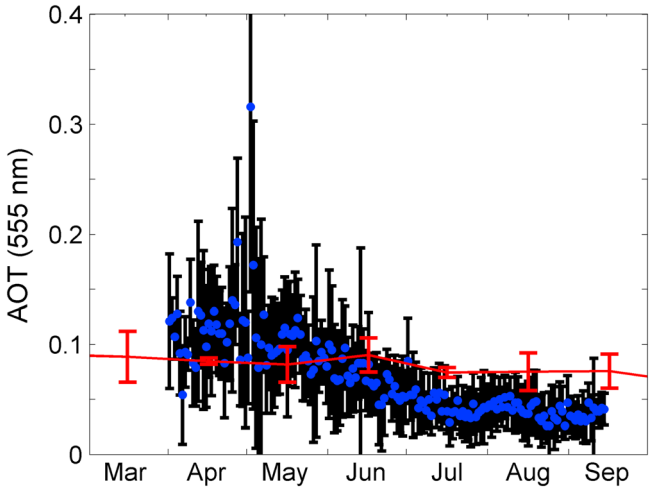

Figure 3. MODIS median column AOTs at 555 nm (blue circles) and corresponding standard deviations (black bars), averaged over the area in Figure 1 and all aerosol pixels corresponding to a day of the year for 9 years (2003–2011) of observations. The red solid line denote CAM4-Oslo global climate model simulation of clear-sky mean AOT, using IPCC AR5 aerosol emissions representative of the years 2006–2008 (discussed in section 3.6).

Norwegian Sea and Barents Sea is much less prominent in summer than in winter. Lower activity in summer in the Svalbard region is also reflected, e.g., in the mean day-to-day absolute change in measured surface pressure in Ny-Ålesund [*Maturilli et al.*, 2013]. However, higher wet removal of accumulation mode particles in summer compared to spring probably also plays a role for the seasonal variation in AOT [*Garrett et al.*, 2011]. The red solid line shown in Figure 3 denotes CAM4-Oslo global climate model simulation of clear-sky mean AOT for the present investigation area (Figure 1). The model results are discussed in section 3.6.

3.3. Stratospheric AOT

To estimate satellite and ground-based tropospheric AOT, aerosol extinction coefficients in the stratosphere have been retrieved based on SAGE III (520/755 nm) and OSIRIS (750 nm) observations (section 2.1.3). Time series of approximate daily mean stratospheric AOT, based on integration of the aerosol extinction coefficient from SAGE III and OSIRIS, are shown in Figure 4 for the periods 2002–2005 and 2002–2011, respectively. The figure also shows SAGE III mean α_{SAGE} (2.02) and a relatively low standard deviation (±0.11) estimated for the period 2002–2005. The α_{SAGE} has been used to estimate OSIRIS and SAGE AOT at the MODIS 555 nm wavelength (black dots and red solid line, respectively). The figure shows good agreement in AOT at 555 nm (on average within 6%) between SAGE III and OSIRIS for the period 2002–2005, with the exception of summer 2002. This deviation may be explained by a difference in latitudinal ranges for which the mean AOT has been estimated. The integration of SAGE III mean aerosol extinction coefficients started at 42°N, while the southernmost latitude is 75°N for the OSIRIS retrievals. The tropopause extends beyond 12 km height at lower latitudes. This means that clouds may have influenced the present SAGE retrievals of AOT during this summer. In addition, Figure 4 shows detection of volcanic aerosols (described in section 3.1) by OSIRIS.

A positive trend in stratospheric background AOT (the volcanic events are excluded) is obtained from both OSIRIS and SAGE III, although the latter operated during a shorter time period. OSIRIS derived AOT at 555 nm shows a statistically significant difference in mean values (at the 99.9% confidence level according to an unpaired *t* test) between the periods 2002–2006 and 2007–2011 (0.0045 ± 0.0014 and 0.0072 ± 0.0008, respectively). Based on observations with several spaceborne instruments, *Vernier et al.* [2011] demonstrated

Table 1. Tropospheric Median Aerosol Optical Thickness and Corresponding Standard Deviation Derived From Spaceborne MODIS Observations and Ground-Based Photometer Measurements for the Period 2003–2011[a]

	AOT (555 nm)		
	2003–2011		
Season	MODIS	AERONET	AWI-AOD
April–May	0.099 ± 0.071 (73%)	0.084 ± 0.051 (40%)	0.068 ± 0.035 (38%)
June	0.063 ± 0.046 (81%)	0.057 ± 0.038 (29%)	0.059 ± 0.028 (36%)
July–August	0.035 ± 0.026 (66%)	0.038 ± 0.025 (15%)	0.035 ± 0.017 (21%)
September	0.031 ± 0.021 (21%)	0.031 ± 0.022 (11%)	0.024 ± 0.052 (11%)

[a]Values were derived for the periods April/May (spring), June (transition), July/August (summer, background), and September (autumn, background). Numbers in parentheses give the data coverage (in percent) for the different platforms and seasons with respect to the whole time period.

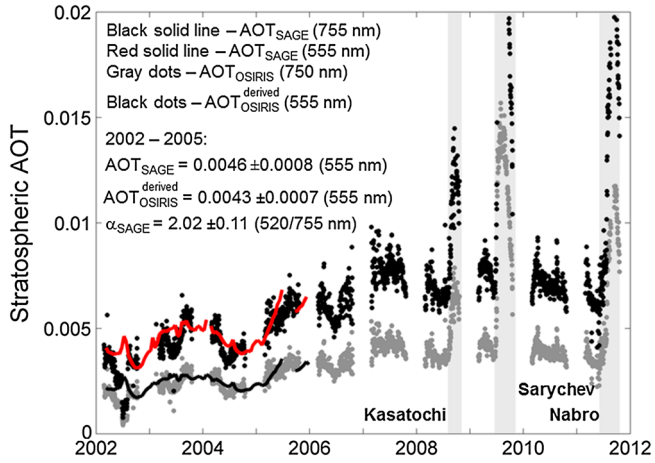

Figure 4. Comparison for the period 2002–2005 between SAGE III and OSIRIS AOT at 755 and 750 nm, respectively, as well as at 555 nm. Black dots denote OSIRIS derived AOT at 555 nm, obtained based on Ångström exponent (α_{SAGE}) from SAGE III AOT (520/755 nm) and OSIRIS AOT at 750 nm for the period 2002–2011. Gray areas indicate time periods for which column AOT over the Svalbard region was influenced by stratospheric volcanic aerosol from 15 August 2008, 3 July 2009, and 12 June 2011, caused by the eruptions of Kasatochi, Sarychev, and Nabro, respectively.

that this trend is mainly driven by a series of moderate but increasingly intense volcanic eruptions that occur primarily at tropical latitudes. These events caused sulfur to be injected directly to altitudes between 18 and 20 km. The aerosol particles that later formed were slowly lofted into the middle stratosphere by the Brewer-Dobson circulation and transported to higher latitudes.

3.4. A Comparison of MODIS AOT Against Ground-Based Measurements

A comparison of median column AOT at 555 nm for the period 2003–2011, retrieved with the MODIS algorithm and measured with AERONET and AWI-AOD Sun photometers, is shown in Figure 5a. Mean values of the Sun photometer measurements have been calculated for comparison with MODIS for days when AOT was retrieved at both the ground-based stations on Svalbard. Otherwise AOT from one of the ground-based stations has been used in the comparison. For these 642 cases the average times (in hours and minutes) and corresponding standard deviations of the observations are $9^{31} \pm 2^{15}$ UTC, $10^{42} \pm 2^{17}$ UTC, and $11^{51} \pm 3^{31}$ UTC for MODIS, AERONET, and AWI-AOD, respectively. The dashed lines shown in Figure 5a represent predicted uncertainties of the MODIS retrievals, i.e., the confidence interval of the MODIS results. The normalized root-mean-square deviation (NRMSD) of 40% was determined for collocated satellite and ground-based daily averaged AOT values (642 in number) according to the procedure described by *Mishchenko et al.* [2010]. In addition, 75% of the satellite values are within the predicted uncertainties of the MODIS retrievals. However, Figure 5a shows that many of the MODIS AOT values are higher than the upper expected uncertainty range of the retrievals. This deviation mainly originates from the heterogeneous aerosol conditions during spring (April and May), as can be seen in Figure 1b, which influences the averaging of the MODIS values, in regard to the relatively large area selected in this study. The time differences between MODIS and AERONET/AWI-AOD observations probably also influence the comparison. For the spring season, 62% of the MODIS values are within the predicted uncertainty of the retrieval, while it is as high as 82% for the months June to beginning of September. In addition, Figures 5b and 5c show relative frequency histograms of MODIS AOT and cumulative distribution curves of MODIS and AEROENET/AWI-AOD AOT, subdivided according to season, of the results in Figure 5a. The difference in median AOT of the cumulative distribution between satellite and ground-based remote sensing is larger for the spring season than for the months June to the beginning of September. When the AERONET and AWI-AOD median AOT values are compared, for 197 days when AOT was retrieved at both ground-based stations during the current 9 year period, a smaller difference between spring and summer is obtained than for MODIS. For spring, cumulative median and standard deviation values of 0.073 ± 0.029 and 0.075 ± 0.032 are obtained for the AERONET and AWI-AOD stations, respectively. For summer no difference in median values is found: 0.051 (±0.025) for AERONET and 0.051 (±0.019) for AWI-AOD. In addition, a NRMSD value of 37% is obtained between the results from AERONET and AWI-AOD for the 197 days when AOT was retrieved at both ground-based stations.

In Table 1 we present MODIS median values for all aerosol pixels in the area shown in Figure 1 for each season and over the 9 year period we have investigated. One satellite scene per day is included for all days for which aerosol data exist. The Sun photometer median values have been obtained in the same way, although for all values produced with respect to the temporal resolution of the measurements. Table 1 shows that for the years 2003–2011, larger differences between MODIS and Sun photometer median

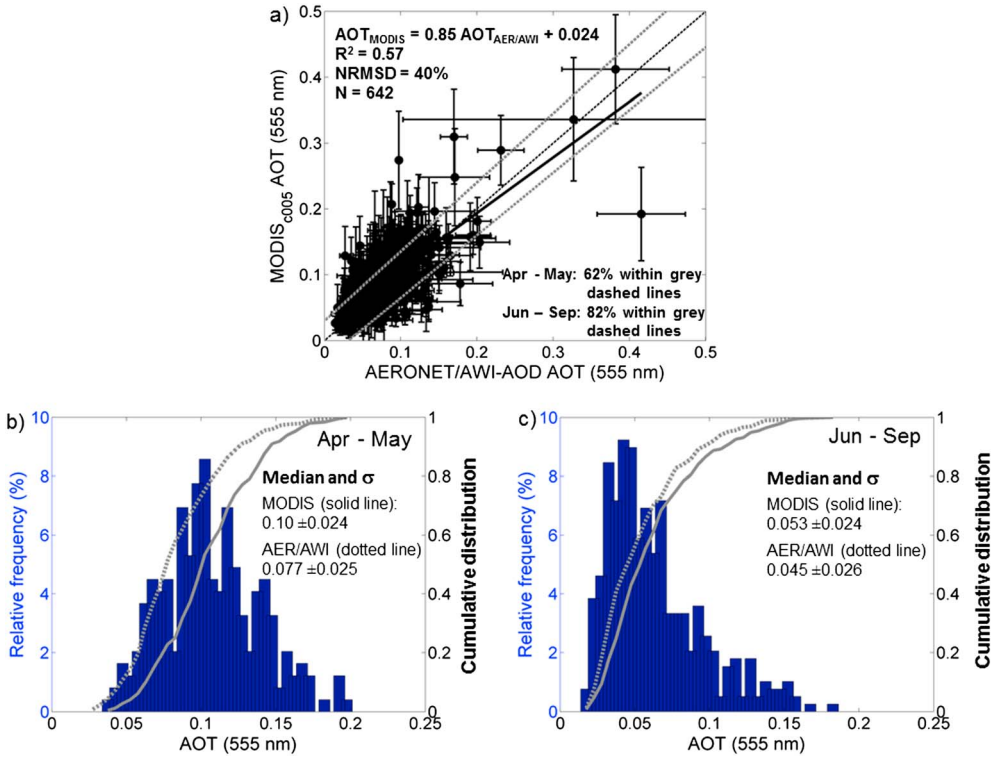

Figure 5. (a) Comparison between MODIS and AERONET/AWI-AOD median column AOTs and the corresponding standard deviations. The black solid, grey dashed, and black dotted lines represent linear fits of the AOT values, expected uncertainties for 1 standard deviation of the MODIS aerosol retrievals, and the 1-to-1 line, respectively. Text at the left top describes the expression for the linear regression curve, coefficient of determination (R^2), normalized root-mean-square deviation (NRMSD), and number of daily coincident measurements (N). Text at the right bottom shows the percentage of the MODIS values that are within the predicted retrievals for the periods April–May and June to the beginning of September. Relative frequency histogram of MODIS AOT (555 nm) and cumulative distribution of MODIS AOT (grey solid line) and AERONET/AWI-AOD AOT (grey dotted line) of the results in Figure 5a, subdivided according to the periods (b) April–May and (c) June–September. Text at the right top in Figures 5b and 5c present results of median and standard deviation (σ) obtained from the cumulative distributions.

tropospheric AOTs are found for spring than for July–September. Note that a significant difference in median tropospheric AOT is also obtained between Sun photometer measurements at Hornsund/Longyearbyen and Ny-Ålesund for spring. Heterogeneous and homogeneous aerosol conditions in spring and summer/autumn, respectively, were also found based on ground-based Sun photometer observations at Ny-Ålesund, Svalbard, in the study by *Stock et al.* [2014]. Furthermore, the tropospheric AOT values in the Table 1 were derived from the total AOT by subtracting the approximate stratospheric AOT from OSIRIS (section 3.3) and by excluding periods associated with influences from biomass-burning and volcanic aerosols (section 3.1), with the exception for the Nabro eruption (13.37°N, 41.70°E), Eritrea, starting at 13 June 2011. Although the latter event highly influenced stratospheric aerosol extinction from about 22 June (Figure 4), relatively modest effects on column AOT are found (Figure 2i). This is explained by deep convection during the monsoon period, which resulted in efficient injection of volcanic sulfur dioxide to the stratosphere before the converted sulfate aerosol were transported toward the Arctic region [*Bourassa et al.*, 2012b]. The tropospheric AOTs corresponding to this period were then included in the present study by subtracting the approximate stratospheric AOT.

Table 1 shows that tropospheric median AOTs from satellite and ground-based measurements are comparable to each other for June and the summer season (July and August), and a relatively small difference in AOT is also found for September. The larger differences found for spring are, thus, partly explained by a spatially inhomogeneous aerosol distribution (Figure 1b). The data coverage for the different platforms for the time period 2003–2011 reveals that MODIS median AOTs are based on substantially better time coverage than the individual ground-based Sun photometer measurements. In addition, the daily data coverage of the

Table 2. Tropospheric Mean Aerosol Optical Thickness and Corresponding Standard Deviation Derived From Spaceborne MODIS Observations and Ground-Based Sun Photometer Measurements for the Period 2003–2011[a]

	AOT (555 nm)			AOT (532 nm)
	2003–2011			1991–1999
Season	MODIS	AERONET	AWI-AOT	AWI-AOT
April–May	0.115 ± 0.069	0.093 ± 0.050	0.075 ± 0.035	0.089 ± 0.033
June	0.072 ± 0.045	0.067 ± 0.037	0.062 ± 0.028	0.051 ± 0.025[b]
July–August	0.041 ± 0.025	0.043 ± 0.024	0.037 ± 0.017	0.044 ± 0.023[b]
September	0.035 ± 0.021	0.038 ± 0.021	0.033 ± 0.052	0.031 ± 0.014

[a]Values were derived for the periods April/May (spring), June (transition), July/August (summer, background), and September (autumn, background). The present results of AOT at 555 nm are compared to mean AOT at 532 nm obtained at Ny-Ålesund, Svalbard, during the period 1991–1999 [*Herber et al.*, 2002].
[b]These values are only presented in this study. *Herber et al.* [2002] reported a mean value of 0.046 (±0.024) for June–August.

observations (AOTs retrieved at least from one of the three platforms in a day), carried out during/over the present investigation period and area, is 80%, 86%, 69%, and 34% for April/May, June, July/August, and September, respectively. For the months July–September the data coverage represents background conditions, since days with influences from biomass burning in 2004 and volcanic aerosols in 2008 and 2009 have been excluded (section 3.1).

3.5. Comparison of Tropospheric AOT Between the Periods 1991–1999 and 2003–2011

Table 2 shows satellite and ground-based tropospheric mean AOT at 555 nm and corresponding standard deviation for the period 2003–2011, compared to tropospheric mean AOT at 533 nm that were obtained at Ny-Ålesund, Svalbard, during the period 1991–1999 [*Herber et al.*, 2002]. The averaging of the present AOT according to season has been carried out in the same way as the results of median AOT in Table 1 (see section 3.4). The table reveals a similar seasonal variation, with substantially higher AOT in spring than in summer, when comparing the two approximate decades. The relatively low difference in AOT between present satellite and ground-based retrievals, as well as compared to AOT obtained in the 1990s for July and August, suggests a relatively small spatial variation in the background tropospheric aerosol load during the Arctic summer.

3.6. Evaluation of Global Climate Model Simulations of AOT

To investigate whether or not the observed column AOT in the Arctic can be simulated with global climate models we have analyzed results obtained with NorESM1-M/CAM4-Oslo (section 2.3). Figure 3 shows somewhat lower CAM4-Oslo AOT for the spring season. This is likely caused by underestimated meridional transport due to underrepresentation of extratropical blocking in the Eurasian-Atlantic sector. As indicated by *Iversen and Joranger* [1985] and more firmly documented by *Iversen* [1989], blocking and high-amplitude planetary waves over Eurasia and the North Atlantic during winter and early spring are closely related to the occurrence of increased levels of particulate sulfate at ground level in Svalbard. Since blocking occurrence was diagnosed to be underrepresented in NorESM by *Iversen et al.* [2013], the winter-spring Arctic haze can be expected to be underestimated. Note that similar errors are found for several models that contribute to CMIP5 [e.g., *Dunn-Sigouin and Son*, 2013; *Masato et al.*, 2013]. Recent investigations indicate that coarse atmospheric model resolution may cause underrepresentation of Euro-Atlantic blocking [*Jung et al.*, 2011; *Dawson et al.*, 2012] as well as storm track activity [*Zappa et al.*, 2013]. Errors in SSTs also cause misrepresentation of blocking [*Scaife et al.*, 2011], which was confirmed for NorESM when the AMIP-runs (based on observed SST) were compared with the fully coupled runs [*Iversen et al.*, 2013]. Nevertheless, the AOT results from CAM4-Oslo shown in Figure 3 for the spring season are within the range of AOT values that were obtained based on observations from the three remote sensing platforms (Table 2). However, the AOT simulated is approximately a factor 2 higher than the MODIS and Sun photometer values for the summer season. The reason for the summer overestimate is less clear than the winter-spring underestimate. One candidate is the vertical transport in deep convective clouds which is likely to be too efficient in the model [*Kirkevåg et al.*, 2013; *Samset et al.*, 2013]. Hence, with the current setup (e.g., with respect to aerosol and precursor emissions, horizontal and vertical model resolution), the model does not reproduce the seasonal variability of the Arctic aerosol, at least not with the observed amplitude.

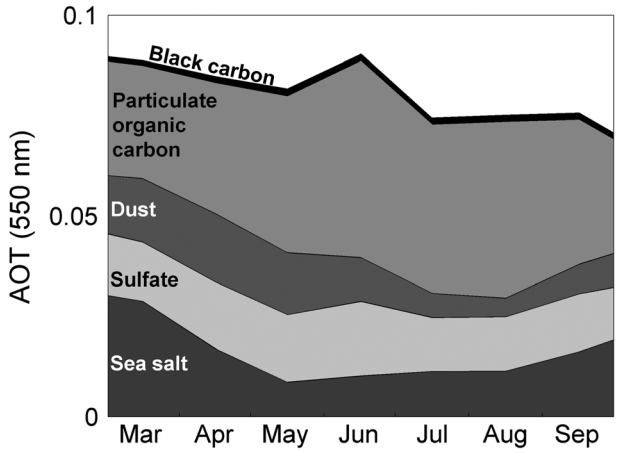

Figure 6. CAM4-Oslo global climate model simulation of AOT in the Svalbard region (75°N–82°N, 10°W–40°E), using greenhouse gas concentrations and IPCC AR5 aerosol emissions representative for the years 2006–2008. The result is subdivided into five chemical aerosol components represented in the model: sea salt, sulfate, dust, particulate organic carbon, and black carbon.

Figure 6 shows the CAM4-Oslo model simulation of AOT in the Svalbard region, subdivided into the five chemical aerosol components represented in the model, with the exception of water from hygroscopic growth (usually not regarded as a separate aerosol constituent). The water uptake is, however, taken into account in the calculation of AOT for each of the other aerosol components. Note that sea salt-related AOT shows a strong seasonal variation—most likely due to its strong connection to surface wind speed, somewhat modulated by its dependence on RH and hygroscopic growth. For particulate organic carbon, both of natural and anthropogenic origins, we find an opposite seasonal variation in AOT. The figure shows that black carbon and particularly dust aerosols of continental origins contribute to AOT also in summer. Furthermore, Figures 7a–7e show the CAM4-Oslo model simulation of vertical profiles of aerosol extinction coefficients in the Svalbard region, for each of the five chemical aerosol components. The figure shows that much of the aerosol extinction related to particulate organic carbon, sulfate, black carbon, and dust aerosols is taking place in the upper free troposphere, which means that long-range transport of aerosols seems to take place in the model also during the summer season. As indicated above this transport is likely exaggerated by the model due to overestimated vertical transport of aerosols and aerosol precursors in deep convective clouds at lower latitudes [*Kirkevåg et al.*, 2013], subsequently leading to overestimated free tropospheric transport of particulate organic carbon, sulfate, black carbon, and dust aerosols to the Arctic region. An influence from distant sources is also suggested from investigations of spatial fields of aerosol concentrations in the model (not shown). For particulate organic carbon, the maximum concentration occurs in late summer and it appears that the aerosols have been transported from lower latitudes, although it is difficult from these analyses (of monthly averaged concentrations) to determine the major source regions. However, for the period 2006–2008 (corresponding to the current simulation period) and investigation area there is no sign of a presence of elevated layers with high extinctions associated with mineral dust or biomass-burning aerosols over the Svalbard area in summer [*Di Pierro et al.*, 2013]. The observations of seasonal mean aerosol extinction profiles have been performed with the CALIPSO lidar. Elevated layers with lower aerosol extinctions in the Arctic can however be difficult to interpret for the summer season due to elevated detection levels and general lower aerosol concentrations [*Di Pierro et al.*, 2013].

The clear seasonal variation in CAM4-Oslo sea salt-related AOT shown in Figure 6 is caused by high wind dependency in the sea spray emissions [*Struthers et al.*, 2011]. This wind dependence is also valid for the emission of primary marine particularly organic carbon in the model [*Kirkevåg et al.*, 2013], and a seasonal variation in AOT also related to this component could be expected. However, the analysis of the model's production of marine secondary organic aerosols reveals enhanced contributions of MSA in the ocean surface layer in summer. Both the maximum in organic aerosol extinction in the lower troposphere (Figure 7b) and the maximum in AOT for June (Figure 6) are probably caused by this effect. Therefore, the overestimation in AOT with nearly a factor of 2 during the summer season may also be influenced by uncertainties in the modeling of marine organic aerosols.

Based on simulations and a limited number of observations and remote sensing data, *Kirkevåg et al.* [2013] suggest that annually averaged AOT is probably overestimated in remote regions at high latitudes in CAM4-Oslo. Note that model-derived annually averaged AOTs at high latitudes in the Southern Hemisphere (70°S–90°S) in that study are somewhat lower than the present AOT observed in summer over the Svalbard area. The model-simulated annually averaged AOT is substantially lower in the Southern Hemisphere than in the Northern Hemisphere, in line with satellite observations [*Kirkevåg et al.*, 2013].

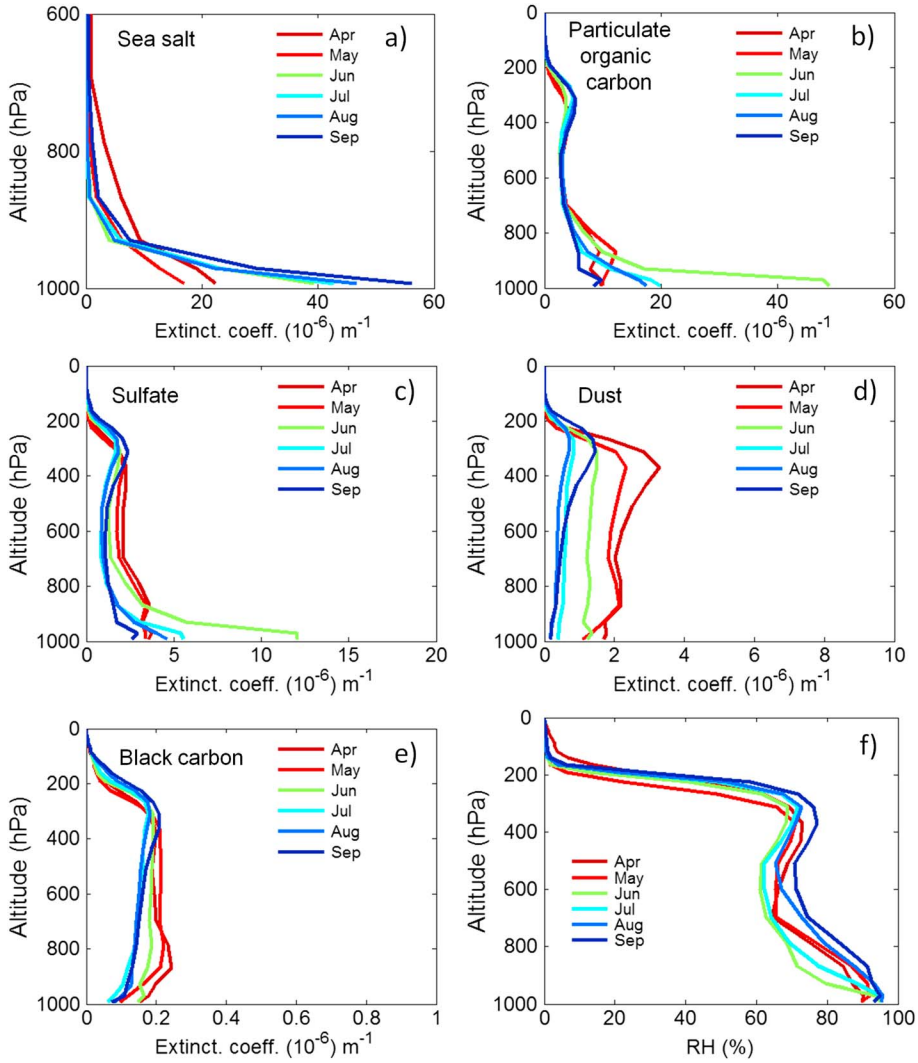

Figure 7. CAM4-Oslo global climate model simulation of all-sky aerosol extinction coefficients in the Svalbard region (75°N–82°N, 10°W–40°E) corresponding to (a) sea salt, (b) particulate organic carbon, (c) sulfate, (d) dust, and (e) black carbon. Figure 7f shows the model-simulated ambient relative humidity (RH).

Figure 7a shows that relatively strong vertical gradients in sea salt-related extinction coefficients are simulated in the lower troposphere, particularly for the months July–September. This may partly be attributed to the large vertical gradients in ambient RH in the lower troposphere, especially in June–August, see Figure 7f. The RH and hygroscopic effect also contributes to the relatively strong gradients in extinction coefficients for particulate organic carbon and sulfate in Figures 7b and 7c. In addition to the influence of hygroscopic growth for all of these components (but not for mineral dust and black carbon), the large extinctions for particulate organic carbon in the lower atmosphere, especially in June (see also the corresponding AOT in Figure 6), may partly be due to too large contributions from MSA for this particular month in the model.

A broader view of the representation of Arctic AOT (for the Svalbard region investigated) in global climate models is provided in Figure 8, which shows average seasonal cycles of all-sky AOT (1980–2004) derived from the CMIP5 model ensemble [*Taylor et al.*, 2012]. The presented subset of CMIP5 models includes only those that have delivered the all-sky AOT for the historical experiment, i.e., an experiment for fully coupled climate models where all known forcings are applied. Information on individual models can be found at http://cmip-pcmdi.llnl.gov/cmip5. Figure 8 reveals large differences between the CMIP5-models and actually a disparity in AOT as large as 1 order of magnitude between some of the models. In addition, several of the CMIP5 models display a weak seasonal variation in AOT, while a reverse seasonal variation,

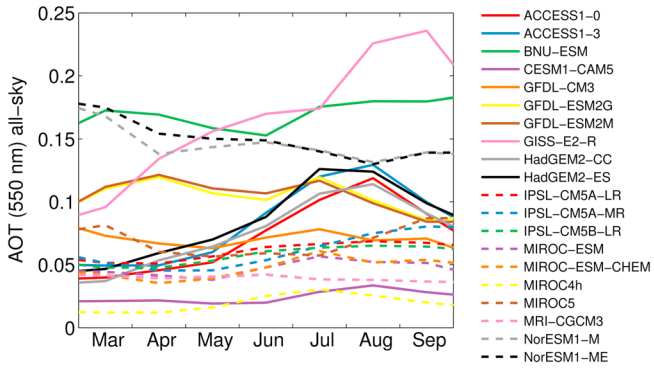

Figure 8. Climatological seasonal cycles of all-sky AOT averaged for the Svalbard area (75°N–82°N, 10°W–40°E) in 20 global climate models participating in the CMIP5 project. The climatological cycles are based on the period 1980–2004 of the CMIP5's "historical" experiment. Information on individual models can be found at http://cmip-pcmdi.llnl.gov/cmip5.

compared to MODIS and ground-based AOT, occurs for several of the models. The overall performance of the models in terms of AOT is poor when compared to the remote sensed data discussed above.

3.7. Comparison Between Tropospheric AOT and Aerosol Scattering Coefficients

In this section we compare observations of the present ambient AOT with current long-term in situ measurements of dry and wet aerosol scattering coefficients at the Zeppelin mountain station. The scattering coefficient is a valid representation of aerosol extinction, at least for the summer season, since the contribution of absorbing aerosols at Svalbard is negligible [*Zieger et al.*, 2010]. The aim is to investigate how representative these in situ measurements are for the Arctic region.

Figure 9 gives a detailed view of the optical and microphysical properties of aerosol particles at the Zeppelin station for 2008. Daily mean DMPS measurements of the dry particle number size distribution measured at the Zeppelin station reveal that spring is dominated by accumulation mode aerosols, while significantly smaller particles are present in summer. This was also found by *Ström et al.* [2003]. A similar conclusion can be drawn from the spatial average of the Ångström exponent (α), derived from the MODIS and Sun photometer observations in the Svalbard region. Figure 9b shows on the whole higher values in summer than in spring. Note that the column α values in late summer of 2008 were influenced by stratospheric aerosol from the Kasatochi volcanic eruption (grey area), which inhibits a comparison of the column α with the ground-based in situ measurements for these days.

Furthermore, Figure 9c shows daily mean RH as well as dry and humidified scattering coefficients at 550 nm obtained for the same seasons of 2008. The ambient scattering coefficients have been derived from dry nephelometer scattering coefficients with respect to RH measured at the Zeppelin station. For the latter parameters, a difference of approximately 1 order of magnitude is found between spring and summer. Events occurring when the station was within clouds (RH $>$ 95%) were excluded in this estimate. An almost equally large difference in dry scattering coefficient between spring and summer has been measured at Barrow, Alaska, during the period 1997–2005 [*Tomasi et al.*, 2007]. In contrast, the seasonal difference in tropospheric mean AOT shown in Table 2 is only about a factor of 2, while it is approximately a factor of 3 for the year 2008 (Figure 2f). A conservative assumption of a mean summertime boundary layer height of 2 km together with vertically homogenous aerosol condition leads to a mean AOT of 0.0022 (±0.0016)—based on the mean extinction value of 1.1 (±0.8 M m^{-1}) measured with the dry nephelometer (RH $<$ 95%) at the Zeppelin station. Such results are consistent with the findings by *Quinn et al.* [2002] at Barrow, Alaska. Thus, the small particles measured with the dry nephelometer in the lower troposphere in summer are inefficient scatterers of light. This is in line with the fact that the mass scattering efficiency at $\lambda = 550$ nm is close to zero for spherical particles smaller than 100 nm in diameter [e.g., *Seinfeld and Pandis*, 1998]. Furthermore, a mean humidified scattering coefficient of 3.68 (±3.76) M m^{-1} is obtained from the results in Figure 9c for July and August 2008. This leads to a mean scattering enhancement factor of 3.3 (±4.2).

In the study by *Zieger et al.* [2010], where a humidified nephelometer was used, a mean scattering enhancement factor of 3.24 ± 0.63 at RH = 85% and $\lambda = 550$ nm, was measured at the Zeppelin station for the period 15 July to 13 October 2008. In addition, the calculated enhancement factor using measured size distribution and assuming a chemistry of ammonium sulfate was found to agree well with the measured enhancement factor [*Zieger et al.*, 2010]. We assume that 50% of the mean tropospheric AOT for summer 2008 is due to aerosols below the altitude of 2 km. Table 3 shows that this results in a mean AOT value of 0.014 (31% daily data coverage) for AWI-AOD at Ny-Ålesund (based on the results shown in Figures 2f and 4).

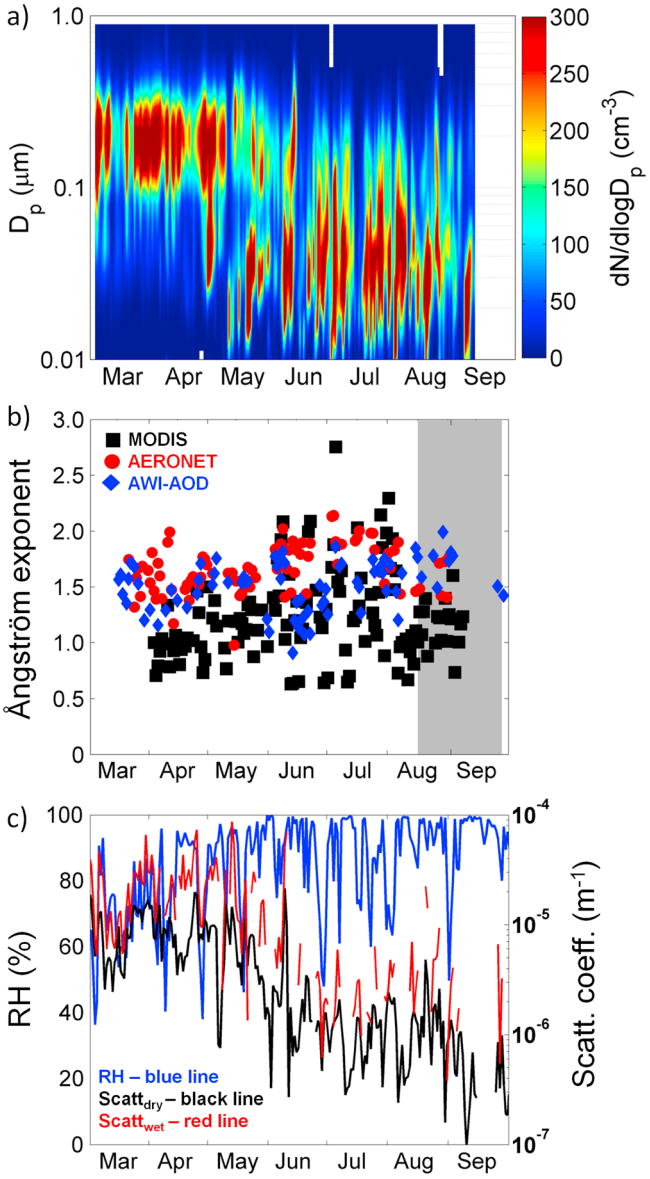

Figure 9. Daily mean values of (a) particle number size distribution (d*N*/dlogD_p) at Zeppelin station, (b) column Ångström exponents obtained with Sun photometers at Svalbard and from MODIS observations in the Svalbard region, and (c) 550 nm scattering coefficient measured with a dry (RH = ~30%) nephelometer (black solid line), humidified scattering coefficient (red solid line) and ambient/outdoor RH (blue solid line) at Zeppelin station, of the year 2008. The shaded area in Figure 9b marks the time period during which column AOT was influenced by the Kasatochi volcano eruption in 2008 (section 3.7).

For AERONET and MODIS mean AOT values of 0.017 (31% daily data coverage) and 0.022 (63% daily data coverage), respectively, are obtained for the same period (Table 3). Note that the simulation of aerosol extinction coefficients corresponding to marine aerosols in CAM4-Oslo support that a majority of the aerosol particles are present in the lower troposphere (see section 3.6 and Figure 7). This means that the mean AOT values of 0.0022 and 0.0075, obtained from dry and humidified scattering coefficients in summer 2008, are at most only 15% and 54%, respectively, of the ambient mean AOT values from remote sensing (Table 3). The relatively large difference found between remote sensing and in situ humidified measurements may be explained, at least partly, by structure in the vertical distribution of the hygroscopic sea-salt aerosol [*Swietlicki et al.*, 2008]. This is further discussed in the following paragraphs.

RH values near 100% in summer suggest that the Zeppelin station is frequently located within clouds. For a further investigation we analyzed daily noon soundings, launched at Ny-Ålesund, with respect to the vertical structure of the lower troposphere. A total of 51 soundings were performed in July and August 2008. Figure 10 shows three typical atmospheric states at the Zeppelin station, in terms of vertical profiles of potential temperature and RH. The station is located within a well-mixed layer when the temperature inversion is present above the height of Zeppelin station. This occurred for 33% of the considered cases. An inversion below the height level of the Zeppelin station indicates that the latter was disconnected from surface influences. This occurred in 28% of the cases. If a RH above 95% is observed at the height level of the Zeppelin station, it can be assumed that the station was inside clouds. This occurred during 29% of the considered cases. The remaining 10% of cases (5 days) refer to cases that are not distinguishable. Thus, the large variations in daily mean scattering coefficient that are measured in summer (Figure 9c) can most likely be explained by variations in the boundary layer height and RH. Inside clouds the nephelometer measures low values of the scattering coefficient due to the low number of interstitial particles. This is because the majority of the accumulation mode particles form cloud droplets during clean conditions [e.g., *Frick and Hoppel*, 1993; *Noone et al.*, 1990]. For the remaining days in summer the daily mean scattering coefficient

Table 3. Lower Tropospheric Ambient Aerosol Optical Thickness (AOT) From Spaceborne MODIS Observations and Ground-Based Sun Photometer Measurements as Well as From Humidified Scattering Coefficients for July and August 2008[a]

	Neph. ($RH_{Zeppelin}$)	Neph. ($RH_{sounding}$)	AWI-AOD	AER	MODIS	AWI/Neph. ($RH_{Zeppelin}$)	AWI/Neph. ($RH_{Sounding}$)
AOT	0.0075 ±0.0077	0.0044 ± 0.0028	0.014 ±0.003	0.017 ± 0.012	0.022 ± 0.012	**1.9 ±2.0**	**3.2 ±2.1**

[a]Dry scattering coefficients measured with a dry nephelometer (Neph.) at the Zeppelin station have been transformed to ambient conditions (see sections 2.2 and 3.7) with respect to RH measured at the Zeppelin station ($RH_{Zeppelin}$) and during sounding ($RH_{sounding}$) by assuming a MBL height of 2 km. Boldface is used to expose the most important results in Table 3.

varies substantially from 1 day to another. Thus, the aerosol sampling was probably performed occasionally in a well-mixed MBL and occasionally above the MBL or surface mixed layer.

Dry scattering coefficients measured at the Zeppelin station in July and August 2008 have been transformed to humidified scattering coefficients with respect to vertical profiles of RH. Only cases for which all the RH values below 2 km are lower than 95% are considered here. This is valid for 16 of the total 51 soundings (26% data coverage) for July and August 2008. Table 3 shows that a mean AOT of 0.0044 is obtained for the 2 km layer when vertical gradients in AOT are accounted for. This is only about 30% of the AWI-AOD AOT.

We have demonstrated that satellite and ground-based ambient AOTs, estimated for the lower troposphere in summer, are substantially larger than ambient AOT estimated for the same layer from humidified scattering coefficients. One reason for this is probably vertical gradients in the marine aerosols in the lower troposphere [*Clarke et al.*, 1996; *Gong et al.*, 1997; *Glantz et al.*, 2004; *Reid et al.*, 2006; *Textor et al.*, 2006; *Lundgren et al.*, 2013]. For the Svalbard area in summer, relatively strong vertical gradients in extinction coefficients for sea salt, particulate organic carbon, and sulfate were also simulated with the CAM4-Oslo global climate model. The assumption of a well-mixed MBL of 2 km in the estimation of Arctic AOT from in

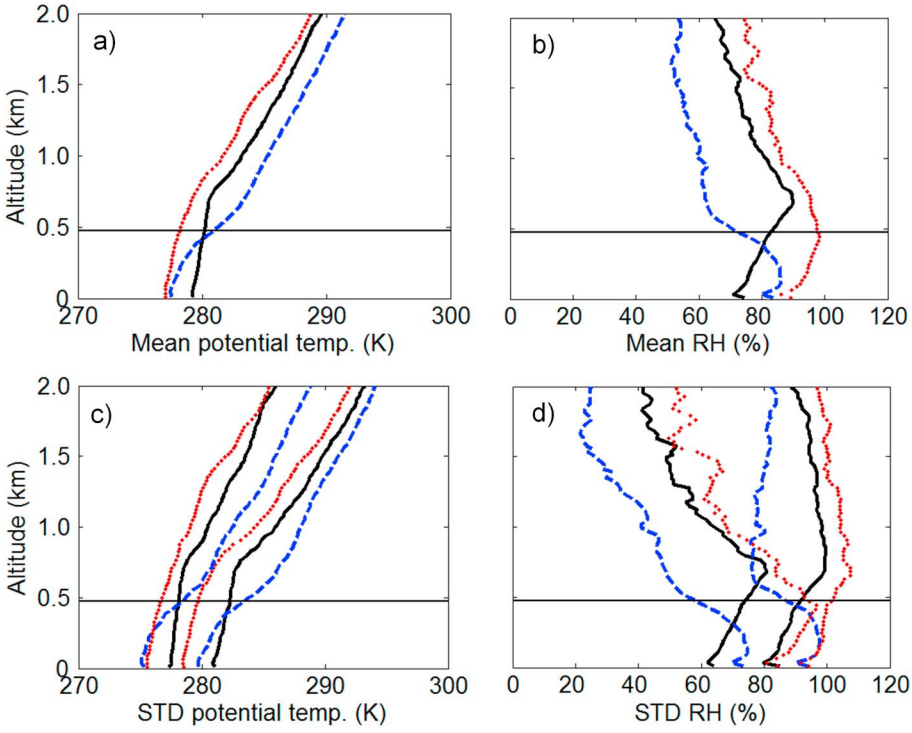

Figure 10. Profiles of (a) mean potential temperature and (c) corresponding 1 standard deviation as well as (b) mean RH and (d) corresponding 1 standard deviation, as obtained from daily noon (12:00 UTC) soundings launched in July and August 2008 at Ny-Ålesund, Svalbard. The horizontal lines denote the height level of the Zeppelin station (474 m). The black solid, blue dashed, and red dotted lines denote mean potential temperature and RH and corresponding 1 standard deviations obtained for days when the Zeppelin station was located within a well-mixed layer, above an inversion and inside clouds, respectively.

situ measurements is a very generous assumption [*Di Pierro et al.*, 2013]. However, a comparison of the dry and humidified nephelometer measurements at RH $< 40\%$ showed that the dry instrument measured about 28% less than the humidified one at the Zeppelin station. Although some hygroscopic growth may be present even at such low RH, one reason for this discrepancy could be losses in the inlet system for the dry nephelometer, due to longer pathways and a lower volumetric flow of 51 min^{-1} than the inlet used for the humidified nephelometer [*Zieger et al.*, 2010].

4. Summary and Conclusions

AOT derived from measurements of MODIS Aqua over the Arctic Ocean have been compared to ground-based Sun photometer measurements performed at Svalbard. The comparison was based on 9 years (2003–2011) of data and the following conclusions have been established:

1. MODIS 555 nm AOTs, for the months April/May and June to the beginning of September, were found to vary within the expected uncertainties of the MODIS retrievals over ocean ($\Delta\text{AOT} = \pm 0.03 \pm 0.05 \cdot \text{AOT}$) for 62% and 82%, respectively, of the compared cases.
2. Values of $R^2 = 0.57$ and NRMSD = 40% were found for 642 of satellite and ground-based daily observations in spring and summer, with a majority of AOT values being lower than 0.15.
3. The standard deviation of 0.025 found for the MODIS retrieval for summer background conditions is acceptable compared to the estimated median AOT of 0.040 (Table 2).

The latter finding in combination with the good agreement to ground-based measurements for the summer season supports the quantitative results obtained with the MODIS algorithm. This also means that AOT retrieved with the MODIS algorithm over ocean and measured with Sun photometer at Svalbard in summer are representative of a relatively large area around Svalbard. For the spring season, however, the differences found between satellite and ground-based AOT are probably due to diverse air masses that cause heterogeneous aerosol conditions in the Svalbard area.

It can be concluded from this study that satellite and ground-based retrievals of AOT in the Arctic marine atmosphere can be of use for validation of regional and global climate models. The following conclusions have been established when evaluating the NorESM/CAM4-Oslo model and the CMIP5 model ensemble against remote sensing of aerosols in the Arctic:

1. The AOT simulated with CAM4-Oslo does not reproduce the observed seasonal variability of Arctic aerosols. The model overestimates AOT by nearly a factor of 2 for the clean background summer season, while the spring maximum is underestimated.
2. A likely contribution to the deviation in summer is an overestimation of transport of aerosols (particulate organic carbon, sulfate, black carbon, and dust) in the free troposphere from midlatitudes to the Arctic. However, the overestimate in AOT may also be influenced by uncertainties in the modeling of marine organic aerosols.
3. The underestimate of AOT in the spring season, although within 1 standard deviation of the retrieved AOD values, is likely influenced by underestimated meridional transport in the Eurasian-Atlantic sector in the atmospheric model. Missing emissions from flaring and a better seasonal variation of midlatitude emissions from domestic heating are other potential contributors [*Sand et al.*, 2013].
4. Large differences in AOT of up to 1 order in magnitude are found for the CMIP5 model ensemble for the spring and summer seasons. Several of the CMIP5 models show a weak seasonal variation in AOT that does not agree with the observations. A reverse seasonal cycle occurs for other CMIP5 models.

Results from in situ measurements of dry and wet aerosol scattering coefficient at the Zeppelin mountain station have been discussed to assess their representativeness for the Arctic region and their usefulness for validation of regional and global climate model simulations of aerosol optical properties. Based on the comparisons with remotely retrieved AOT in the ambient atmosphere, the following conclusions have been established:

1. A difference as large as a mean factor of 7 in summer was obtained between satellite/ground-based ambient AOT and AOT estimated from dry nephelometer measurements for the lower troposphere in the Svalbard region.
2. A decoupled marine boundary layer develops occasionally over the ocean area around Svalbard in summer and is likely to cause vertical gradients in marine aerosol mass concentrations and extinction coefficients,

which are further enhanced by hygroscopic growth. This is in line with the finding of substantially larger satellite and ground-based ambient AOTs (with at least a mean factor of 1.9) estimated for the lower troposphere, compared to estimates based on in situ measurements at the Zeppelin station. Therefore, we conclude that factors such as hygroscopic growth, vertical aerosol gradients, and the frequent occurrence of fog and clouds have crucial effects on the representativeness of aerosol measurements at the Zeppelin station for the Arctic MBL in summer.

In the present study tropospheric AOT has been estimated based on satellite and ground-based remote sensing. A better picture of the optical properties of aerosols in the Arctic marine lower atmosphere can be obtained by adding a Sun photometer to the measurement setup at the Zeppelin mountain station. Such an instrument at the elevated site in combination with other ground-based Sun photometers at Svalbard will be useful to characterize AOT within the lower troposphere. These measurements were originally planned to begin in spring 2013.

Acknowledgments

We thank the PIs of the AERONET sites used in this study for maintaining their stations. We acknowledge the MODIS mission scientists and associated NASA personnel for the production of the data used in this research effort. The authors are also thankful for the use of ECMWF data sets. We acknowledge the World Climate Research Programme's Working Group on Coupled Modeling, which is responsible for CMIP, and we thank the climate modeling groups for producing and making their model output available. The work was financed through research grants from the Swedish Research Council for the Environment, Agricultural Sciences and Spatial Planning (FORMAS). Furthermore, we thank the Norwegian Space Center for funding NILU received for the SatMonAir project (NSC nr: JOP.12.12.2), as well as the funding MET Norway received through the PM-VRAE project. T. Iversen, A. Kirkevåg, and Ø. Seland were supported by the Research Council of Norway through the EarthClim (207711/E10) and NOTUR/NorStore projects, and through the EU projects PEGASOS and ACCESS. We thank the CRAICC project for their work on initiating cooperation on Nordic Arctic climate modeling and measurements. The authors are very thankful for the use of in situ aerosol data that are measured by the Department of Applied Environmental Science (ITM) at Stockholm University. The authors would like to thank Ulla Wideqvist at ITM for useful suggestions. Finally, we also want to thank three anonymous reviewers for their valuable comments.

References

Arctic Climate Impact Assessment (2005), Impacts of a Warming Arctic: Arctic Climate Impact Assessment (ACIA), *Tech. Rep.*, 140 pp., Cambridge Univ. Press, Cambridge.

Anderson, T. L., and J. A. Ogren (1998), Determining aerosol radiative properties using the TSI 3563 integrating nephelometer, *Aerosol Sci. Technol.*, *29*, 57–69.

Ångström, A. (1964), The parameters of atmospheric turbidity, *Tellus*, *16*, 64–75.

Bentsen, M., et al. (2013), The Norwegian Earth System Model, NorESM1-M—Part 1: Description and basic evaluation of the physical climate, *Geosci. Model Dev.*, *6*, 687–720, doi:10.5194/gmd-6-687-2013.

Bodhaine, B. A. (1989), Barrow surface aerosol—1976–1986, *Atmos. Environ.*, *23*, 2357–2369.

Bodhaine, B. A., J. M. Harris, and G. A. Herbert (1981), Aerosol light-scattering and condensation nuclei measurements at Barrow, Alaska, *Atmos. Environ.*, *15*, 1375–1389.

Bourassa, A. E., D. A. Degenstein, R. L. Gattinger, and E. J. Llewellyn (2007), Stratospheric aerosol retrieval with OSIRIS limb scatter measurements, *J. Geophys. Res.*, *112*, D10217, doi:10.1029/2006JD008079.

Bourassa, A. E., D. A. Degenstein, and E. J. Llewellyn (2008), SASKTRAN: A spherical geometry radiative transfer code for efficient estimation of limb scattered sunlight, *J. Quant. Spectros. Radiat. Transfer*, *109*, 52–73.

Bourassa, A. E., L. A. Rieger, N. D. Lloyd, and D. A. Degenstein (2012a), Odin-OSIRIS stratospheric aerosol data product and SAGE III intercomparison, *Atmos. Chem. Phys.*, *12*, 605–614, doi:10.5194/acp-12-605-2012.

Bourassa, A. E., A. Robock, W. J. Randel, T. Deshler, L. A. Rieger, N. D. Lloyd, E. J. (Ted) Llwellyn, and D. A. Degenstein (2012b), Large volcanic aerosol load in the stratosphere linked to Asian monsoon transport, *Science*, *337*, 78–81, doi:10.1126/science.1219371.

Bretherton, C. S., P. Austin, and S. T. Siems (1995), Cloudiness and marine boundary layer dynamics in the ASTEX Lagrangian Experiments. Part II: Cloudiness, drizzle, surface fluxes and entrainment, *J. Atmos. Sci.*, *52*, 2724–2735.

Clarke, A. D., T. Uehara, and J. N. Porter (1996), Lagrangian evolution of an aerosol column during the Atlantic Stratocumulus Transition Experiment, *J. Geophys. Res.*, *101*(D2), 4351–4362, doi:10.1029/95JD02612.

Dawson, A., T. N. Palmer, and S. Corti (2012), Simulating regime structures in weather and climate prediction models, *Geophys. Res. Lett.*, *39*, L21805, doi:10.1029/2012GL053284.

Deweaver, E. T., and C. M. Bitz (2006), Atmospheric circulation and its effect on Arctic sea ice in CCSM3 simulations at medium and high resolution, *J. Clim.*, *19*, 2415–2436.

Di Pierro, M., L. Jaeglé, E. W. Eloranta, and S. Sharma (2013), Spatial and seasonal distribution of Arctic aerosols observed by the CALIOP satellite instrument (2006–2012), *Atmos. Chem. Phys.*, *13*, doi:10.5194/acp-13-7075-2013.

Dunn-Sigouin, E., and S.-W. Son (2013), Northern Hemisphere blocking frequency and duration in the CMIP5 models, *J. Geophys. Res. Atmos.*, *118*, 1179–1188, doi:10.1002/jgrd.50143.

Engvall, A. -C., R. Krejci, J. Ström, R. Treffeisen, R. Scheele, O. Hermansen, and J. Paatero (2008), Changes in aerosol properties during spring-summer period in the Arctic troposphere, *Atmos. Chem. Phys.*, *8*, 445–462.

Frick, G. M., and W. A. Hoppel (1993), Airship measurements of aerosol size distributions, cloud droplet spectra, and trace gas concentrations in the marine boundary layer, *Bull. Am. Meteorol. Soc.*, *70*, 354–365.

Gao, B.-C., J. Yoram, Y. J. Kaufman, D. Tanre, and R.-R. Li (2002), Distinguishing tropospheric aerosols from thin cirrus clouds for improved aerosol retrievals using the ratio of 1.38-μm and 1.24-μm channels, *Geophys. Res. Lett.*, *29*(18), 1890, doi:10.1029/2002GL015475.

Garrett, T. J., S. Brattstrom, S. Sharma, D. E. J. Worthy, and P. Novelli (2011), The role of scavenging in the seasonal transport of black carbon and sulfate to the Arctic, *Geophys. Res. Lett.*, *38*, L16805, doi:10.1029/2011GL048221.

Gent, P. R., et al. (2011), The Community Climate System Model version 4, *J. Clim.*, *24*, 4973–4991, doi:10.1175/2011JCLI4083.1.

Glantz, P., and M. Tesche (2012), Assessment of two aerosol optical thickness retrieval algorithms applied to MODIS Aqua and Terra data in Europe, *Atmos. Meas. Tech.*, *5*, 1727–1740.

Glantz, P., G. Svensson, K. J. Noone, and S. R. Osborne (2004), Sea-salt aerosols over the Northeast Atlantic: Model simulations of ACE-2 2nd Lagrangian experiment, *Quart. J. Roy. Meteorol. Soc.*, *130*, 2191–2215.

Glantz, P., D. E. Nilsson, and W. von Hoyningen-Huene (2009), Estimating a relationship between aerosol optical thickness and surface wind speed over the ocean, *Atmos. Res.*, *92*(1), 58–68.

Gong, S. L., L. A. Barrie, and J. P. Blanchet (1997), Modeling sea-salt aerosols in the atmosphere 1. Model development, *J. Geophys. Res.*, *102*, 3805–3818, doi:10.1029/96JD02953.

Hack, J. J., J. M. Caron, G. Danabasoglu, K. W. Oleson, C. M. Bitz, and J. E. Truesdale (2006), CCSM–CAM3 climate simulation sensitivity to changes in horizontal resolution, *J. Clim.*, *19*, 2267–2289.

Herber, A., L. W. Thomason, H. Gernandt, U. Leiterer, D. Nagel, K. Schulz, J. Kaptur, T. Albrecht, and J. Notholt (2002), Continuous day and night aerosol optical depth observations in the Arctic between 1991 and 1999, *J. Geophys. Res.*, *107*(D10), 4097, doi:10.1029/2001JD000536.

Hoffmann, A., C. Ritter, M. Stock, M. Maturilli, S. Eckhardt, A. Herber, and R. Neuber (2010), Lidar measurements of the Kasatochi aerosol plume in August and September 2008 in Ny-Ålesund, Spitsbergen, *J. Geophys. Res.*, *115*, D00L12, doi:10.1029/2009JD013039.

Holben, B. N., et al. (1998), AERONET e a federated instrument network and data archive for aerosol characterization, *Remote Sens. Environ.*, *66*(1), 1–16.

Hurrell, J. W., J. J. Hack, A. S. Phillips, J. Caron, and J. Yin (2006), The dynamical simulation of the Community Atmosphere Model Version 3 (CAM3), *J. Clim.*, *19*, 2162–2183.

Istomina, L. G., W. von Hoyningen-Huene, A. A. Kokhanovsky, E. Schultz, and J. P. Burrows (2011), Remote sensing of aerosols over snow using infrared AATSR observations, *Atmos. Meas. Tech.*, *4*, 1133–1145, doi:10.5194/amt-4-1133-2011.

Iversen, T. (1989), Some statistical properties of ground level air pollution at Norwegian Arctic stations and their relation to large scale atmospheric flow systems, *Atmos. Environ.*, *23*, 2451–2462.

Iversen, T., and E. Joranger (1985), Arctic air pollution and large scale atmospheric flow, *Atmos. Environ.*, *19*, 2099–2108.

Iversen, T., et al. (2013), The Norwegian Earth System Model, NorESM1- M—Part 2: Climate response and scenario projections, *Geosci. Model Dev.*, *6*, 389–415, doi:10.5194/gmd-6-389-2013.

Johnson, D. W., et al. (2000), Observations of the evolution of the aerosol, cloud and boundary layer characteristics during the 1st ACE-2 Lagrangian experiment, *Tellus*, *52B*, 348–376.

Jung, T., et al. (2011), High-resolution global climate simulations with the ECMWF Model in project Athena: Experimental design, model climate, and seasonal forecast skill, *J. Clim.*, *25*, 3155–3172.

Kahn, R. A., M. J. Garay, D. L. Nelson, R. C. Levy, M. A. Bull, D. J. Diner, J. V. Martonchik, E. G. Hansen, L. Remer, and D. Tanré (2011), Response to "Toward unified satellite climatology of aerosol properties," 3. MODIS versus MISR versus AERONET, *J. Quant. Spectros. Radiat. Transfer*, *112*, 901–909.

Kent, G. S., M. P. McCormick, and P. H. Wang (1994), Validation of Stratospheric Aerosol and Gas Experiments I and II satellite aerosol optical depth measurements using surface radiometer data, *J. Geophys. Res.*, *99*, 10,333–10,339, doi:10.1029/94JD00167.

Kirkevåg, A., and T. Iversen (2002), Global direct radiative forcing by process-parameterized aerosol optical properties, *J. Geophys. Res.*, *107*, 4433, doi:10.1029/2001JD000886.

Kirkevåg, A., et al. (2013), Aerosol-climate interactions in the Norwegian Earth System Model—NorESM1-M, *Geosci. Model Dev.*, *6*, 207–244, doi:10.5194/gmd-6-207-2013.

Lamarque, J.-F., et al. (2010), Historical (1850–2000) gridded anthropogenic and biomass burning emissions of reactive gases and aerosols: Methodology and application, *Atmos. Chem. Phys.*, *10*, 7017–7039, doi:10.5194/acp-10-7017-2010.

Levy, R. C., L. A. Remer, R. G. Kleidman, S. Mattoo, C. Ichoku, R. Kahn, and T. F. Eck (2010), Global evaluation of the Collection 5 MODIS dark-target aerosol products over land, *Atmos. Chem. Phys.*, *10*, 10,399–10,420, doi:10.5194/acp-10-10399-2010.

Lewis, E. R., and S. E. Schwartz (2004), *Sea Salt Aerosol Production: Mechanisms, Methods, Measurements and Models: A Critical Review*, p. 413, AGU, Washington, D. C.

Llewellyn, E. J., et al. (2004), The OSIRIS instrument on the Odin spacecraft, *Can. J. Phys.*, *82*(6), 411–422.

Lundgren, K., B. Vogel, H. Vogel, and C. Kottmeier (2013), Direct radiative effects of sea salt for the Mediterranean region under conditions of low to moderate wind speeds, *J. Geophys. Res. Atmos.*, *118*, 1906–1923, doi:10.1029/2012JD018629.

Martins, J., D. Tanre, L. Remer, Y. Kaufman, S. Mattoo, and R. Levy (2002), MODIS Cloud screening for remote sensing of aerosols over oceans using spatial variability, *Geophys. Res. Lett.*, *29*(12), 1619, doi:10.1029/2001GL013252.

Masato, G., B. J. Hoskins, and T. Woollings (2013), Winter and summer Northern Hemisphere blocking in CMIP5 models, *J. Clim.*, *26*, 7044–7059, doi:10.1175/JCLI-D-12-00466.1.

Maturilli, M., A. Herber, and G. König-Langlo (2013), Climatology and time series of surface meteorology in Ny-Ålesund, Svalbard, *Earth Syst. Sci. Data*, *5*, 155–163, doi:10.5194/essd-5-155-2013.

Mazzola, M., et al. (2012), Evaluation of sun photometer capabilities for retrievals of aerosol optical depth at high latitudes: The POLAR-AOD intercomparison campaigns, *Atmos. Environ.*, *52*, 4–17.

Meehl, G. A., et al. (2012), Climate system response to 13 external forcings and Climate Change Projections in CCSM4, *J. Clim.*, *25*, 3661–3683, doi:10.1175/JCLI-D-11-00240.1.

Mei, L., Y. Xue, A. A. Kokhanovsky, W. von Hoyningen-Huene, L. Istomina, G. de Leeuw, J. P. Burrows, J. Guang, and Y. Jing (2013a), Aerosol optical depth retrieval over snow using AATSR data, *Int. J. Remote Sens.*, *24*(14), 5030–5041.

Mei, L., Y. Xue, G. de Leeuw, W. von Hoyningen-Huene, A. A. Kokhanovsky, L. Istomina, J. Guang, and J. P. Burrows (2013b), Aerosol optical depth retrieval in the Arctic region using MODIS data over snow, *Remote Sens. Environ.*, *128*, 234–245.

Mishchenko, M., L. Liu, I. V. Geogdzhayev, L. D. Travis, B. Cairns, and A. A. Lacis (2010), Toward unified satellite climatology of aerosol properties. 3. MODIS versus MISR versus AERONET, *J. Quant. Spectros. Radiat. Transfer*, *111*, 540–552.

Mulcay, J. P., C. D. O'Dowd, S. D. Jennings, and D. Ceburnus (2008), Significant enhancement of aerosol optical depth in marine air under high wind conditions, *Geophys., Res. Lett.*, *35*, L16810, doi:10.1029/2008GL034303.

Murtagh, D., et al. (2002), Review: An overview of the Odin atmospheric mission, *Can. J. Phys.*, *80*, 309–319.

Myhre, C. L., et al. (2007), Regional aerosol optical properties and radiative impact of the extreme smoke event in the European Arctic in spring 2006, *Atmos. Chem. Phys.*, *7*, 511–534.

Neale, R. B., et al. (2010), Description of the NCAR Community Atmosphere Model (CAM 4.0), *Tech. Note NCAR/TN-485+STR*, Natl. Cent. for Atmos. Res., Boulder, Colo.

Nicholls, S. (1984), The dynamics of stratocumulus: Aircraft observations and comparisons with a mixed layer model, *Q. J. R. Meteorol. Soc.*, *110*, 783–820.

Nilsson, E. D., Ü. Rannik, E. Swietlicki, C. Leck, P. P. Aalto, J. Zhou, and M. Norman (2001), Turbulent aerosol fluxes over the Arctic Ocean: 2. Winddriven sources from the sea, *J. Geophys. Res.*, *106*, 32,111–32,124, doi:10.1029/2000JD900426.

Noone, K. J., J. A. Ogren, and J. Heintzenberg (1990), An examination of clouds at a mountain-top site in central Sweden: The distribution of solute within cloud droplets, *Atmos. Res.*, *25*, 3–15.

Osborne, S. M., et al. (2000), Evolution of the aerosol, cloud and boundary layer dynamic and thermodynamic characteristics during the second Lagrangian experiment of ACE-2, *Tellus*, *52B*, 375–400.

Pacyna, J., and B. Ottar (1985), Transport and chemical composition of the summer aerosol in the Norwegian Arctic, *Atmos. Environ.*, *19*(12), 2109–2120.

Pierce, J. R., and P. J. Adams (2006), Global evaluation of CCN formation by direct emission of sea salt and growth of ultrafine sea salt, *J. Geophys. Res.*, *111*, D06203, doi:10.1029/2005JD006186.

Quinn, P. K., T. L. Miller, T. S. Bates, J. A. Ogren, E. Andrews, and G. E. Shaw (2002), A 3-year record of simultaneously measured aerosol chemical and optical properties at Barrow, Alaska, *J. Geophys. Res.*, *107*(D11), 4130, doi:10.1029/2001JD001248.

Reid, J. S., B. Brooks, K. K. Crahan, D. A. Hegg, T. F. Eck, N. O'Neill, G. de Leeuw, E. A. Reid, and K. D. Anderson (2006), Reconciliation of coarse mode sea-salt aerosol particle size measurements and parameterizations at a subtropical ocean receptor site, *J. Geophys. Res.*, *111*, D02202, doi:10.1029/2005JD006200.

Remer, L. A., et al. (2005), The MODIS aerosol algorithm, products, and validation, *J. Atmos. Sci.*, *62*, 947–973.

Russell, P. B., and M. P. McCormick (1989), SAGE II aerosol data validation and initial data use: An introduction and overview, *J. Geophys. Res.*, *94*, 8335–8338, doi:10.1029/JD094iD06p08335.

Scaife, A. A., D. Copsey, C. Gordon, C. Harris, T. Hinton, S. Keeley, A. O'Neill, M. Roberts, and K. Williams (2011), Improved Atlantic winter blocking in a climate model, *Geophys. Res. Lett.*, *38*, L23703, doi:10.1029/2011GL049573.

Stratospheric Aerosol and Gas Experiment III Algorithm Theoretical Basis Document (2002), SAGE III Algorithm Theoretical Basis Document: Solar and Lunar Algorithm, Earth Observing System Project science Office web site online. [Available at http://eospso.gsfc.nasa.gov.]

Samset, B. H., et al. (2013), Black carbon vertical profiles strongly affect its radiative forcing uncertainty, *Atmos. Chem. Phys.*, *13*, 2423–2434.

Sand, M., T. K. Berntsen, Ø. Seland, and J. E. Kristjánsson (2013), Arctic surface temperature change to emissions of black carbon within Arctic or midlatitudes, *J. Geophys. Res. Atmos.*, *118*, 7788–7798, doi:10.1002/jgrd.50613.

Seinfeld, J. H., and S. N. Pandis (1998), *Atmospheric Chemistry and Physics*, John Wiley, New York.

Seland, Ø., T. Iversen, A. Kirkevåg, and T. Storelvmo (2008), Aerosol-climate interactions in the CAM-Oslo atmospheric GCM and investigation of associated basic shortcomings, *Tellus*, *60A*, 459–491, doi:10.1111/j.1600--0870.2008.00318.x.

Serreze, M. C., and P. Barrett (2008), The summer cyclone maximum over the Central Arctic Ocean, *J. Clim.*, *21*, 1048–1065, doi:10.1175/2007JCLI1810.1.

Smirnov, A., B. N. Holben, T. F. Eck, O. Dubovik, and I. Slutsker (2000), Cloud screening and quality control algorithms for the AERONET database, *Remote Sens. Environ.*, *73*, 337–349.

Smirnov, A., et al. (2012), Effect of wind speed on aerosol optical depth over remote oceans, based on data from Maritime Aerosol Network, *Atmos. Meas. Tech.*, *5*, 377–388.

Stock, M., C. Ritter, V. Aaltonen, W. Aas, D. Handorff, A. Herber, R. Treffeisen, and K. Dethloff (2014), Where does the optically detectable aerosol in the European Arctic come from?, *Tellus B*, *2014*(66), 21,450.

Stohl, A., et al. (2006), Pan-Arctic enhancements of light absorbing aerosol concentrations due to North American, boreal forest fires during summer 2004, *J. Geophys. Res.*, *111*, D22214, doi:10.1029/2006JD007216.

Stohl, A., et al. (2007), Arctic smoke—Record high air pollution levels in the European Arctic due to agricultural fires in Eastern Europe, *Atmos. Chem. Phys.*, *7*, 511–534.

Stroeve, J. C., V. Kattsov, A. Barrett, M. Serreze, T. Pavlova, M. Holland, and W. N. Meier (2012), Trends in Arctic sea ice extent from CMIP5, CMIP3 and observations, *Geophys. Res. Lett.*, *39*, L16502, doi:10.1029/2012GL052676.

Stroeve, J., M. M. Holland, W. Meier, T. Scambos, and M. Serreze (2007), Arctic sea ice decline: Faster than forecast, *Geophys. Res. Let.*, *34*, L09501, doi:10.1029/2007GL029703.

Ström, J., J. Umegård, K. Tørseth, P. Tunved, H.-C. Hansson, K. Holmén, V. Wismann, A. Herber, and G. König-Langlo (2003), One year of particle size distribution and aerosol chemical composition measurements at the Zeppelin station, Svalbard, March 2000–March 2001, *Phys. Chem. Earth*, *28*, 1181–1190.

Struthers, H., A. M. L. Ekman, P. Glantz, T. Iversen, A. Kirkevåg, E. M. Mårtensson, Ø. Seland, and E. D. Nilsson (2011), The effect of sea ice loss on sea salt aerosol concentrations and the radiative balance of the Arctic, *Atmos. Chem. Phys.*, *11*, 3459–3477.

Swietlicki, E., et al. (2008), Hygroscopic properties of submicrometer atmospheric aerosol particles measured with H-TDMA instruments in various environments – A review, *Tellus B*, *60*, 432–469.

Taylor, K. E., R. J. Stouffer, and G. A. Meehl (2012), An overview of CMIP5 and the experiment design, *Bull. Am. Meteorol. Soc.*, *93*, 485–498, doi:10.1175/BAMS-D-11-00094.1.

Textor, C., et al. (2006), Analysis and quantification of the diversities of aerosol life cycles within AeroCom, *Atmos. Chem. Phys.*, *6*, 1777–1813.

Thomason, L. W., J. R. Moore, M. C. Pitts, J. M. Zawodny, and E. W. Chion (2010), An evaluation of SAGE III version 4 aerosol extinction coefficient and water vapor products, *Atmos. Chem. Phys.*, *10*, 2159–2173.

Toledano, A. (2012), Overview of sun photometer measurements of aerosol properties in Scandinavia and Svalbard, *Atmos. Env.*, *52*, 18–28.

Tomasi, C., et al. (2007), Aerosols in polar regions: A historical overview based on optical depth and in situ observations, *J. Geophys. Res.*, *112*, D16205, doi:10.1029/2007JD008432.

Tomasi, C., et al. (2012), An update on polar aerosol optical properties using POLAR-AOD and other measurements performed during the International Polar Year, 52, *Atmos. Env.*, *52*, 29–47.

Treffeisen, R., R. Krejci, J. Ström, A. C. Engvall, A. Herber, and L. Thomason (2007a), Humidity observations in the Arctic troposphere over Ny-Ålesund, Svalbard based on 15 years of radiosonde data, *Atmos. Chem. Phys.*, *7*, 2721–2732.

Treffeisen, R., et al. (2007b), Arctic smoke—Aerosol characteristics during a record smoke event in the European Arctic and its radiative impact, *Atmos. Chem. Phys.*, *7*, 3035–3053.

Vernier, J.-P., et al. (2011), Major influence of tropical volcanic eruptions on the stratospheric aerosol layer during the last decade, *Gephys. Res. Lett.*, *38*, L12807, doi:10.1029/2011GL047563.

Weinbruch, S., D. Wiesemann, M. Ebert, K. Schütze, R. Kallenborn, and J. Ström (2012), Chemical composition and sources of aerosol particles at Zeppelin Mountain (Ny Ålesund, Svalbard): An electron microscopy study, *Atmos. Env.*, *49*, 142–150.

Wood, R., et al. (2000), Boundary layer and aerosol evolution during the 3rd Lagrangian experiment of ACE-2, *Tellus*, *52B*, 239–257.

Zappa, G., L. C. Shaffrey, and K. I. Hodges (2013), The ability of CMIP5 models to simulate North Atlantic Extratropical Cyclones, *J. Clim.*, *26*, 5379–5396, doi:10.1175/JCLI-D-12-00501.1.

Zhang, J., R. Lindsay, A. Schweiger, and M. Steele (2012), The impact of an intense summer cyclone on 2012 Arctic sea ice retreat, *Geophys. Res. Lett.*, *40*, 720–726, doi:10.1002/grl.50190.

Zieger, P., R. Fierz-Schmidhauser, M. Gysel, J. Ström, S. Henne, K. E. Yttri, U. Baltensberger, and E. Weingartner (2010), Effects of relative humidity on aerosol light scattering in the Arctic, *Atmos. Chem. Phys.*, *10*, 3875–3890.